Response to review comments on acp-2016-453

The original comments are provided in black, our response is given in red.

The authors show that WRF-Chem with the physical and chemical schemes chosen for their study has substantial biases at 60 km horizontal resolution over eastern North America. The biases depend only weakly on the cumulus scheme or lateral boundary conditions. At 12 km horizontal resolution the biases to re-analysis data, in particular for precipitation, are smaller. The intended quantification of the value added by enhanced resolution in the description of the drivers of aerosol direct radiative forcing over eastern North America cannot be achieved with the current setup as the bias in precipitation implies a bias in wet scavenging (the most important removal mechanism for aerosol particles, as mentioned in the study) and the bias in boundary layer humidity leads to biases in aerosol water uptake and therefore AOD (which is discussed in the study).

Therefore either the focus of the manuscript needs to be changed to discuss the performance of WRF-Chem at different horizontal resolutions in general or the setup needs to be changed for example by running a simulation with 36 km horizontal resolution. Only then can publication be considered.

The reviewer indicated in his/her review: "the focus of the manuscript needs to be changed to discuss the performance of WRF-Chem at different horizontal resolutions in general or the setup needs to be changed for example by running a simulation with 36 km horizontal resolution."

Given that we are already seeking to synthesize 5 sets of year-long simulations in a single manuscript, in response to this comment we have modified the manuscript to include a more balanced description of the performance of WRF-Chem at different horizontal resolutions in terms of the meteorological, gas-phase and aerosol properties (and have changed the title to reflect this refocus). A tracked changes version of the manuscript is attached that shows all of the changes we have made.

The impact of resolution on meteorological, chemical and aerosol properties in ~~Value-added by high-resolution~~ regional simulations with WRF-Chem ~~simulations of climate-relevant aerosol properties~~

P. Crippa[1], R. C. Sullivan[2], A. Thota[3], S. C. Pryor[2,3]

[1]COMET, School of Civil Engineering and Geosciences, Cassie Building, Newcastle University, Newcastle upon Tyne, NE1 7RU, UK

[2]Department of Earth and Atmospheric Sciences, Bradfield Hall, 306 Tower Road, Cornell University, Ithaca, NY 14853, USA

[3]Pervasive Technology Institute, Indiana University, Bloomington, IN 47405, USA

Correspondence to: P. Crippa (paola.crippa@ncl.ac.uk), School of Civil Engineering and Geosciences, Cassie Building, Room G15, Telephone: +44 (0)191 208 5041, Newcastle University, Newcastle upon Tyne, NE1 7RU, UK

Abstract

~~Despite recent advances in global Earth System Models (ESMs), the current global mean aerosol direct and indirect radiative effects remain uncertain, as does their future role in climate forcing and regional manifestations. Reasons for this uncertainty include the high spatio-temporal variability of aerosol populations. Thus, limited area (regional) models applied at higher resolution over specific regions of interest are generally expected to 'add value', i.e. improve the fidelity of the physical-dynamical-chemical processes that induce extreme events and dictate climate forcing, via more realistic representation of spatio-temporal variability. However, added value is not inevitable, and there remains a need to optimize use of numerical resources, and to quantify the impact on simulation fidelity that derives from increased resolution.~~ Limited area (regional) models applied at high resolution over specific regions of interest are generally expected to more accurately capture the spatio-temporal variability of key meteorological and climate parameters. However, ~~added value~~~~their~~ improved performance is not inevitable, and there remains a need to optimize use of numerical resources, and to quantify the impact on simulation fidelity that derives from increased resolution. The application of regional models for climate forcing assessment is currently limited by the lack of studies quantifying ~~their performance as a function of~~ the sensitivity to horizontal spatial resolution and ~~of~~ the physical-dynamical-chemical schemes driving the simulations. Here we ~~quantify~~ investigate ~~the sensitivity of~~ model skills ~~on spatial resolution value added by enhanced spatial resolution~~ in simulati~~ons~~ng ~~of~~ meteorological, chemical and aerosol properties as a function of spatial resolution, ~~the drivers of aerosol direct radiative forcing~~ by applying the Weather Research and Forecasting model with coupled Chemistry (WRF-Chem) over eastern North America at different resolutions. Using Brier Skill Scores and other statistical metrics it is shown that enhanced resolution (from 60 to 12 km) improves model performance for all of the meteorological parameters and gas phase concentrations considered, in addition to both mean and extreme Aerosol Optical Depth (AOD) in three wavelengths in the visible relative to satellite observations, principally via increase of potential skill. Some of the enhanced model performance for AOD appears to be attributable to improved simulation of ~~specific humidity and the resulting impact on aerosol hygroscopic growth/hysteresis.~~ meteorological conditions (notably precipitation and near-surface specific humidity) and the concentration of key aerosol precursor gases (e.g. SO_2 and NH_3).

Keywords: added value, high-resolution WRF-Chem simulations, precipitation, aerosol optical properties, extreme AOD

1 Motivation and Objectives

Aerosols alter Earth's radiation balance primarily by scattering or absorbing incoming solar radiation (direct effect, dominated by accumulation mode (diameters ~ wavelength (λ), where total extinction is often quantified using AOD), or regulating cloud formation/properties by acting as cloud condensation nuclei (CCN) (indirect effect, dominated by diameters ≥ 100 nm, magnitude = f(composition)). Most aerosols (excluding black carbon) have a larger scattering cross-section than absorption cross-section, and act as CCN thus enhancing cloud albedo and lifetimes. Hence increased aerosol concentrations are generally (but not uniformly) associated with surface cooling (offsetting a fraction of greenhouse gas warming) (Boucher, 2013;Myhre et al., 2013b) to a degree that is principally dictated by the aerosol concentration, size and composition, in addition to the underlying surface and height of the aerosol layer (McComiskey et al., 2008). Despite major advances in measurement and modeling, both the current global mean aerosol direct effect (possible range: -0.77 to +0.23 W m^{-2}) and the indirect effect (possible range: -1.33 to -0.06 W m^{-2}) remain uncertain (Stocker, 2013), as does their future role in climate forcing (Rockel et al., 2008) and regional manifestations (Myhre et al., 2013a). Specific to our current study region (eastern N. America), one analysis using the NASA GISS global model found that the "regional radiative forcing from US anthropogenic aerosols elicits a strong regional climate response, cooling the central and eastern US by 0.5–1.0 °C on average during 1970–1990, with the strongest effects on maximum daytime temperatures in summer and autumn. Aerosol cooling reflects comparable contributions from direct and indirect radiative effects" (Leibensperger et al., 2012). A recent comparison of multiple global models conducted under the AEROCOM-project indicated this is also a region that exhibits very large model-to-model variability in simulated AOD (<AOD> ~ 0.5, σ(AOD) ~ 1) (Myhre et al., 2013a).

Major reasons why aerosol radiative forcing on both the global and regional scales remains uncertain include short atmospheric residence times and high spatio-temporal variability of aerosol populations, and the complexity of the processes that dictate aerosol concentrations, composition and size distributions (Seinfeld and Pandis, 2016). Although aerosol processes and properties are increasingly being treated in the global Earth System Models (ESMs) (Long et al., 2015;Tilmes et al., 2015) ~~being~~ applied in the Coupled Model Intercomparison Project Phase 6 (CMIP-6) (Meehl et al., 2014), the scales on which such models are applied remain much coarser than those on which aerosol population properties are known to vary (Anderson et al., 2003). Therefore, limited area atmospheric models (regional models) applied at higher resolution over specific regions of interest are expected to 'add value' (i.e. improve the fidelity) of the physical-dynamical-chemical processes that induce extreme events and dictate climate forcing. There is empirical evidence to suggest a strong resolution dependence in simulated aerosol particle properties. For example, WRF-Chem simulations with spatial resolution enhanced from 75 km to 3 km exhibited higher correlations and lower bias relative to observations of aerosol optical properties over Mexico likely due to more accurate description of emissions, meteorology and of the physicochemical processes that convert trace gases to particles (Gustafson et al., 2011;Qian et al., 2010). This improvement in the simulation of aerosol optical properties implies a reduction of the uncertainty in associated aerosol radiative forcing (Gustafson et al., 2011). Further, WRF-Chem run over the United Kingdom and Northern France at multiple resolutions in the range of 40-160 km, underestimated AOD by 10-16% and overestimated CCN by 18-36% relative to a high resolution run at 10 km, partly as a result of scale dependence of the gas-phase chemistry and differences in the aerosol uptake of water (Weigum et al., 2016)~~ (Weigum et al., 2016)~~.

However, debate remains regarding how to objectively evaluate model performance, quantify the value added by enhanced resolution (Di Luca et al., 2015;Rockel et al., 2008) and on possible limits to the improvement of climate representation in light of errors in the driving "imperfect lateral boundary conditions" (Diaconescu and Laprise, 2013). Nevertheless, although "it is unrealistic to expect a vast amount of added values since models already performs rather decently" (Di Luca et al., 2015) and global ESMs are now run at much higher resolution than in the past, it is generally assumed that high resolution regional models will add value via more realistic representation of spatio-temporal variability than global coarser-resolution simulations. Further, "the main added value of a regional climate model is provided by its small scales and its skill to simulate extreme events, particularly for precipitation" (Diaconescu and Laprise, 2013).

It is particularly challenging to assess the added-value from enhanced resolution in the context of climate-relevant aerosol properties since they are a complex product of the fidelity of the simulation of meteorological parameters, gas-phase precursors, emissions and the treatment of aerosol dynamics. Here we quantify the value added by enhanced resolution in the description of ~~the drivers of~~~~meteorological~~ physical and chemical atmospheric conditions~~aerosol direct radiative forcing~~ using year-long simulations from WRF-Chem over eastern North America, and investigate how they impact AOD~~ representation~~. The primary performance evaluation of aerosol properties focuses on AOD at different wavelengths (λ = 470, 550 and 660 nm, where the AOD at different λ is used as a proxy of the aerosol size distribution (Tomasi et al., 1983), see details in Sect. 2.~~1~~3) and is measured relative to observations from satellite-borne instrumentation. Thus the term "value-~~-~~added" is used here in the context of columnar aerosol properties to refer to an improvement of model performance in simulation of wavelength specific AOD as measured by the MODerate resolution Imaging Spectroradiometer (MODIS) instrument aboard the polar-orbiting Terra satellite. To attribute sources of the enhanced fidelity of AOD, our analysis also incorporates evaluation of the value-added by enhanced resolution in terms of key meteorological and gas-phase drivers of aerosol concentrations and composition and is conducted relative to the MERRA-2 reanalysis product for the physical variables and columnar gas concentrations from satellite observations (see details of the precise data sets used given below). The meteorological parameters considered are air temperature at 2 m (T_{2m}), total monthly precipitation (*PPT*), planetary boundary-layer height (*PBLH*) and specific humidity in the boundary layer (Q_{PBL}). The gas phase concentrations considered are sulfur dioxide (SO_2), ammonia (NH_3), nitrogen dioxide (NO_2) and formaldehyde (HCHO).

We begin by quantifying the performance of WRF-Chem when applied over eastern North America at a resolution of 60 km (WRF60) (~ finest resolution likely to be employed in CMIP-6 global simulations) and then compare the results to those from simulations conducted at 12 km (WRF12) (simulation details are given in Table 1). Quantification of model skill is undertaken by mapping the WRF12 output to the WRF60 grid (WRF12-remap) and computing Brier Skill Scores (BSS) using MODIS as the target, WRF60 as the reference forecast and WRF12-remap as the forecast to be evaluated. We also evaluate the performance of the WRF-Chem simulations of 2008 relative to climatology as represented by MODIS observations for 2000-2014. We additionally assess the impact of simulation resolution on extreme AOD values that are associated with enhanced impacts on climate and human health. This analysis uses both *Accuracy* and *Hit Rate* as the performance metrics and focuses on the co-occurrence of extreme values in space from the model output and MODIS.

~~To attribute sources of added value, O~~~~our analysis also incorporates evaluation of the value-added by enhanced resolution in terms of key meteorological and gas-phase drivers of aerosol concentrations and composition and is conducted relative to the MERRA-2 reanalysis product for the physical variables and columnar gas concentrations from satellite observations (see details of the precise data sets used given below). The meteorological parameters considered are air temperature at 2 m (T_{2m}), total monthly precipitation (PPT), planetary boundary-layer height (PBLH) and specific humidity in the boundary layer (Q_{PBL}). The gas phase~~

~~concentrations considered are:~~are ~~sulfur dioxide (SO_2), ammonia (NH_3), nitrogen dioxide (NO_2) and formaldehyde (HCHO).~~

Based on the performance evaluation of the WRF-Chem simulations that indicate substantial dry bias in the WRF60 simulations and large seasonality in the ~~value added~~ skill-scores for AOD ~~by~~ as a function of ~~enhanced~~ resolution, we conducted two further year-long simulations at 60 km. In the first we held all other simulation conditions constant but selected a different cumulus parameterization. In the second, we held all simulation conditions constant but employed a different set of lateral boundary conditions for the meteorology. In the context of the precipitation biases reported herein it is worthy of note that discrepancies in simulated precipitation regimes are key challenges in regional modelling (both physical and coupled with chemistry). Although the Grell 3D scheme has been successfully applied in a number of prior analysis wherein the model was applied at resolutions in the range of 1-36 km (e.g. (Grell and Dévényi, 2002;Lowrey and Yang, 2008;Nasrollahi et al., 2012;Sun et al., 2014;Zhang et al., 2016)), the North American Regional Climate Change Assessment Program (NARCCAP) simulations with WRF at 50-km were also dry biased in the study domain (Mearns et al., 2012). Although there have been a number of studies that have sought to evaluate different cumulus schemes over different regions at different resolutions, no definitive recommendation has been made regarding the dependence of model~~'s~~ skill on resolution and cumulus parameterization (Arakawa, 2004;Jankov et al., 2005;Nasrollahi et al., 2012;Li et al., 2014). ~~Thus~~Hence, further research is needed to identify the optimal cumulus scheme for use over North America at coarser resolution. Thus, we performed a sensitivity analysis on the cumulus scheme at 60 km by applying the Grell-Freitas parameterization (Grell and Freitas, 2014), which is the next generation of the Grell 3D scheme.

2 Materials and Methods

~~2.1 Spectral dependence of AOD~~[PC1]

~~Three properties dictate the actual aerosol direct radiative forcing: AOD, single scattering albedo and asymmetry factor, all of which are a function of the wavelength (λ) of incident radiation. The first property is related to the total columnar mass loading, typically dominates the variability of direct aerosol effect (Chin et al., 2009) and is the focus of the current research. The relationship between the aerosol size distribution and spectral dependence of AOD is described by a power law function:~~

$$\cancel{\beta(\lambda_1) = \beta(\lambda_2) \times \left(\frac{\lambda_1}{\lambda_2}\right)^{-\alpha}} \quad \text{~~(1)~~}$$

~~where β is the particle extinction coefficient at a specific wavelength λ, and α is the Ångström exponent (Ångström, 1964) which describes the wavelength dependence of AOD (and is inversely proportional to the average aerosol diameter):~~

$$\cancel{\alpha = \frac{ln\frac{AOD(\lambda_1)}{AOD(\lambda_2)}}{ln\frac{\lambda_2}{\lambda_1}}} \quad \text{~~(2)~~}$$

~~The aerosol volume distribution usually conforms to a multi-lognormal function with n modes:~~

$$\cancel{\frac{dV(r)}{d\ln r} = \sum_{i=1}^{n} \frac{C_i}{\sqrt{2\pi}\sigma_i} \exp\left[\frac{-(\ln r - \ln R_i)^2}{2\sigma_i^{\ 2}}\right]} \quad \text{~~(3)~~}$$

~~where r is the particle radius and C_i, R_i and σ_i are the particle volume concentration, the geometric mean radius and the standard deviation in the mode i respectively.~~

~~We can thus compute AOD for a polydisperse distribution of aerosols with refractive index m in an atmospheric column of height Z as:~~

$$\cancel{AOD(\lambda) = \int \frac{3\beta(m,r,\lambda)}{4r} \frac{dV(r)}{d\,ln\,r} d\,ln\,r dZ} \quad \text{~~(4)~~}$$

~~**As indicated in (Schuster et al., 2006), "the spectral variability of extinction diminishes for particles larger than the incident wavelength", thus fine mode particles contribute more to AOD in the visible (λ~0.5 µm) than at longer wavelengths, whereas coarse mode particles provide a similar AOD both at short and long wavelengths. This is reflected in the Ångström parameter which can be thus used as a proxy for the fine mode fraction or fine mode radius (Schuster et al., 2006).**~~

2.1~~2~~ WRF-Chem simulations

WRF-Chem (version 3.6.1) simulations were performed for the calendar year 2008 over eastern North America, in a domain centered over southern Indiana (86°W, 39°N) at two resolutions, one close to the finest resolution designed for CMIP-6 global model runs (i.e. 60 km, WRF60) and the other one at much higher resolution (12 km, WRF12). Simulation settings are identical for the two runs except for the time-step used for the physics (Table 1). Physical and chemical parameterizations were chosen to match previous work using WRF-Chem at 12 km on the same region which showed good performance relative to observations and the year 2008 was selected because it is representative of average climate and aerosol conditions during 2000 - 2014 (Crippa et al., 2016). More specifically the simulations adopted the RADM2 chemical mechanism (Stockwell et al., 1990) and a modal representation of the aerosol size distribution (MADE/SORGAM, (Ackermann et al., 1998;Schell et al., 2001)) with three lognormal modes and fixed geometric standard deviations (i.e. 1.7, 2 and 2.5 for Aitken, accumulation and coarse mode, respectively (Ackermann et al., 1998;Grell et al., 2005)). Aerosol direct feedback was turned on and coupled to the Goddard shortwave scheme (Fast et al., 2006). A telescoping vertical grid with 32 model layers from the surface to 50 hPa and 10 layers up to 800 hPa was selected. Meteorological initial and boundary conditions from the North American Mesoscale Model at 12 km resolution (NAM12) are applied every 6 hours, while initial and chemical boundary conditions are taken from MOZART-4 (Model for Ozone and Related chemical Tracers, version 4) with meteorology from NCEP/NCAR-reanalysis (Emmons et al., 2010). Anthropogenic emissions are specified for both WRF60 and WRF12 from the US National Emission Inventory 2005 (NEI-05) (US-EPA, 2009) which provides hourly point and area emissions at 4 km on 19 vertical levels. The simulation settings and specifically the use of a modal representation of the aerosol size distribution were selected to retain computational tractability. Accordingly, the 60 km simulations for the year 2008 completed in 6.4 hours whereas the 12 km simulations completed in 9.5 days (230 hours) on the Cray XE6/XK7 supercomputer (Big Red II) owned by Indiana University, using 256 processors distributed on 8 nodes.

As described in detail below, in the WRF60 simulations configured as described in Table 1, simulated precipitation during the summer months exhibits substantial dry bias, and the analysis of value added by enhanced simulation resolution exhibited strong seasonality. We performed a sensitivity analysis to the cumulus scheme, by conducting an additional year-long simulation at 60 km using the Grell-Freitas parameterization (Grell and Freitas, 2014), which is an evolution of Grell 3D that is scale-aware and treats some aspects of aerosol-cloud interactions. We also tested the sensitivity of the simulation results to the meteorological boundary conditions, by repeating the WRF60 simulations using output from the Global Forecast System (GFS) at 0.5° resolution every 6 hours to provide the lateral boundary conditions.

~~Value added is quantified using Brier Skill Scores (BSS) and is evaluated in two ways: first by evaluating the model performance as a function of simulation resolution and then using climatology as the reference 'forecast'. In these analyses the hourly output from the 12 km resolution simulation is degraded (averaged) to 60 km (hereafter WRF12-remap) as follows: the 12 km domain is resized excluding 2 grid cells at the border to exactly match the 60 km resolution domain. Each coarse grid cell thus includes 5×5 12 km resolution cells and its value is the mean of all valid 12 km grid cells inside it if at least half of those cells contain valid AOD (i.e. no cloud cover), otherwise the whole coarse cell is treated as missing. In all comparisons only cells with simultaneous (i.e. model and MODIS) clear sky conditions are considered. A daily value from WRF-Chem is computed as an instantaneous value for the hour nearest to the satellite overpass time. When the comparison is done on a monthly basis, a monthly mean value is computed from the daily values obtained under clear sky conditions, only if there are at least five valid observations in the month.~~

2.2~~3~~ Observations

Model aerosol optical properties are evaluated relative to the MODIS Collection 6 dark-target land aerosol product from aboard the Terra satellite (~1030 overpass local solar time (LST)) (Levy et al., 2013). To provide a consistent assessment of model skill, the evaluation of AOD is conducted only on land areas since the MODIS dark-target ocean aerosol product is based on a retrieval algorithm different from the one over land (Levy et al., 2013). Trace gas concentrations are evaluated relative to measurements from the Ozone Monitoring Instrument (OMI; version 3) (Chance, 2002) and the Infrared Atmospheric Sounding Interferometer (IASI; NN version 1) (Whitburn et al., 2016) aboard the Aura (~1345 LST) and MetOp satellites (~0930 LST), respectively. MODIS retrieves AOD at multiple λ including 470, 550, and 660 nm, and the MODIS algorithm removes cloud-contaminated pixels prior to spatial averaging over 10 × 10 km (at nadir). OMI and IASI have nadir resolutions of 13 × 24 km and 12 km (circular footprint), respectively, and have been filtered to remove retrievals with cloud fractions > 0.3 (Fioletov et al., 2011;McLinden et al., 2014;Vinken et al., 2014) and OMI pixels affected by the row anomalies. MODIS, OMI, and IASI provide near daily global coverage, although the row anomalies render portions of the OMI viewing swath unusable. Uncertainty in AOD from MODIS is spatially and temporally variable. It has been estimated as ± (0.05 + 15%) for AOD over land (Levy et al., 2013), and prior research has reported 71% of MODIS Collection 5 retrievals fall within 0.05 ± 20% for AOD relative to AERONET in the study domain (Hyer et al., 2011). The accuracy of OMI ("root sum of the square of all errors, including forward model, inverse model, and instrument errors" (Brinksma et al., 2003)) is 1.1 DU or 50% for SO_2, 2×10^{14} cm^{-2}/30% for background/polluted NO_2 conditions, and 35% for HCHO. This uncertainty is typically reduced by spatial and temporal averaging, as employed herein (Fioletov et al., 2011;Krotkov et al., 2008). IASI NH_3 retrievals do not use an a priori assumption of emissions, vertical distribution, or lifetime of NH_3 (i.e. no averaging kernel); therefore, NH_3 accuracy is variable (Whitburn et al., 2016), and thus only retrievals with uncertainty lower than the retrieved concentrations are used herein.

For the model evaluation, satellite observations for each day are regridded to the WRF-Chem discretization. This is done by averaging all valid retrievals within: 0.1° and 0.35° of the WRF-Chem grid-cell center for the 12×12 km and 60×60 km resolutions, respectively for MODIS; 0.125° × 0.18° (along-track/latitudinal × cross-track/longitudinal) and 0.365° × 0.42° for OMI; 0.12° and 0.36° for IASI. To avoid issues from under-sampling, we require at least 10 valid MODIS granules for the 60×60 km daily average to be computed and at least 5 daily averages to compute a monthly average for each grid cell. Model evaluation of gaseous species is performed on a seasonal basis using standard scores (z-scores), which are computed as the difference between the seasonal mean within a grid cell and the seasonal spatial mean, divided by the seasonal spatial standard deviation. Use of z-scores allows comparison of the spatial patterns of satellite observations and model output in terms of standard deviation units from the mean.

The simulated meteorological properties are evaluated using Modern-Era Retrospective analysis for Research and Applications (MERRA-2) reanalysis data as the target. MERRA-2 is a homogenized and continuous in time description of atmospheric properties on a 3-dimensional global grid (horizontal resolution of 0.5°×0.625°, L72), developed by NASA and was released in Fall 2015 (Molod et al., 2015). MERRA-2 provides hourly values of T_{2m} and *PBLH*, and vertical profile of 3-dimensional variables every 3 hours on a large number of pressure levels. Here we compute the total specific humidity (Q_{PBL}) of the lowest 8 pressure levels (i.e. in the boundary-layer approximated as the layer from 1000 to 825 hPa) in MERRA-2, assuming an average air density in the PBL of 1.1 kg m^{-3}. For the evaluation of simulated precipitation we use accumulated monthly total values.

~~2.4~~ 2.3~~1~~ Spectral dependence of AOD

Three properties dictate the actual aerosol direct radiative forcing: AOD, single scattering albedo and asymmetry factor, all of which are a function of the wavelength (λ) of incident radiation. The first property is related to the total columnar mass loading, typically dominates the variability of direct aerosol effect (Chin et al., 2009) and is the focus of the current research. The relationship between the aerosol size distribution and spectral dependence of AOD is described by a power law function:

$$\beta(\lambda_1) = \beta(\lambda_2) \times \left(\frac{\lambda_1}{\lambda_2}\right)^{-\alpha} \quad (1)$$

where β is the particle extinction coefficient at a specific wavelength λ, and α is the Ångström exponent (Ångström, 1964) which describes the wavelength dependence of AOD (and is inversely proportional to the average aerosol diameter):

$$\alpha = \frac{ln \dfrac{AOD(\lambda_1)}{AOD(\lambda_2)}}{ln \dfrac{\lambda_2}{\lambda_1}} \quad (2)$$

The aerosol volume distribution usually conforms to a multi-lognormal function with n modes:

$$\frac{dV(r)}{d\ln r} = \sum_{i=1}^{n} \frac{C_i}{\sqrt{2\pi}\sigma_i} \exp\left[\frac{-(\ln r - \ln R_i)^2}{2\sigma_i^2}\right] \quad (3)$$

where r is the particle radius and C_i, R_i and σ_i are the particle volume concentration, the geometric mean radius and the standard deviation in the mode i respectively.

We can thus compute AOD for a polydisperse distribution of aerosols with refractive index m in an atmospheric column of height Z as:

$$AOD(\lambda) = \int \frac{3\beta(m,r,\lambda)}{4r} \frac{dV(r)}{d\ln r} d\ln r\, dZ \quad (4)$$

As indicated in (Schuster et al., 2006), “the spectral variability of extinction diminishes for particles larger than the incident wavelength”, thus fine mode particles contribute more to AOD in the visible (λ~0.5 μm) than at longer wavelengths, whereas coarse mode particles provide a similar AOD both at short and long wavelengths. This is reflected in the Ångström parameter which can be thus used as a proxy for the fine mode fraction or fine mode radius (Schuster et al., 2006).

2.4 Quantification of model performance and added-value

Taylor diagrams summarize three aspects of model performance relative to a reference: the spatial correlation coefficient (i.e. Pearson correlation of the fields, r), the ratio of spatial standard deviations of the two spatial fields ($\sigma_{wrf}/\sigma_{sat}$) and the root mean squared difference (RMSD) (Taylor, 2001). Here Taylor diagrams are presented for monthly mean AOD from WRF60, WRF12 and WRF12-remap relative to MODIS at different wavelengths (Fig. 1 d-f). Because AOD is not normally distributed, Spearman's rank correlation coefficients (ρ) of the mean monthly AOD spatial fields are also computed to reduce the impact of a few outliers and the small sample size during cold months (Table 2~~Table 2~~). To assess the significance of ρ while accounting for multiple testing, we apply a Bonferroni correction (Simes, 1986) in which for m hypothesis tests, the null hypothesis is rejected if $p \leq \frac{\alpha}{m}$, where p is the p-value and α is the confidence level (0.05 is used here).

We further quantify the value added (or lack of thereof) of the high-resolution simulations using the following metrics:

(i) Brier Skill Score

Value added is quantified using Brier Skill Scores (BSS) and is evaluated in two ways: first by evaluating the model performance as a function of simulation resolution and then using climatology as the reference 'forecast'. In these analyses the hourly output from the 12 km resolution simulation is degraded (averaged) to 60 km (hereafter WRF12-remap) as follows: the 12 km domain is resized excluding 2 grid cells at the border to exactly match the 60 km resolution domain. For example, in the analysis of AOD e~~E~~ach coarse grid cell thus includes 5×5 12 km resolution cells and its value is the mean of all valid 12 km grid cells inside it if at least half of those cells contain valid AOD (i.e. no cloud cover), otherwise the whole coarse cell is treated as missing. In all comparisons of AOD only cells with simultaneous (i.e. model and MODIS) clear sky conditions are considered. A daily value from WRF-Chem is computed as an instantaneous value for the hour nearest to the satellite overpass time. When the comparison is done on a monthly basis, a monthly mean value is computed from the daily values obtained under clear sky conditions, only if there are at least five valid observations in the month.

The primary metric used to quantify the added value of WRF12-remap versus WRF60 is the Brier Skill Score (BSS) (Murphy and Epstein, 1989):

$$BSS = \frac{r_{F'P'}^{2} - \left(r_{F'P'} - \frac{\sigma_{F'}}{\sigma_{P'}} \right)^{2} - \left(\frac{\langle P' \rangle - \langle F' \rangle}{\sigma_{P'}} \right)^{2} + \left(\frac{\langle P' \rangle}{\sigma_{P'}} \right)^{2}}{1 + \left(\frac{\langle P' \rangle}{\sigma_{P'}} \right)^{2}} \quad \textbf{(5)}$$

where F is the "forecast" (i.e. the 12 km simulations mapped to 60 km, WRF12-remap); P is the "target" (i.e. for AOD this is MODIS at 60 km) and output from WRF60 are used as the reference forecast; F' the difference between 12 km estimates regridded to 60 km and MODIS; P' the difference between the 60 km simulation and the 'target' (i.e. for the AOD MODIS observations regridded to 60 km). In the analysis of BSS relative to the long-term (15-year) climatology of AOD from MODIS, the monthly mean climatological value of AOD is used as the reference forecast, while WRF60 and WRF12-remap are used as the forecasts, and monthly mean AOD from MODIS at 60 km is the target.

BSS measures by how much a test simulation (WRF12-remap) more closely (or poorly) reproduces observations (from MODIS, MERRA-2 or other satellite products) relative to a control (WRF60) run. For example, a BSS>0 indicates WRF12, even when regridded to 60 km, does add value. The first term in (5) ranges from 0 to 1, is described as the potential skill, and is the square of the spatial correlation coefficient between forecast and reference anomalies to MODIS. It is the skill score achievable if both the conditional bias (second term) and overall bias (third term) were zero, and for most of the variables considered herein (particularly AOD) it contributes to a positive BSS in most calendar months (and seasons). The second term (the conditional bias, > 0), is the square of the difference between the anomaly correlation coefficient and the ratio of standard deviation of the anomalies and is small if for all points F' is linear to P'. The third term is referred to as the forecast anomaly bias, and is the ratio of the difference between the mean anomalies of WRF12-remap and the observations relative to WRF60 and the standard deviation of WRF60 anomaly relative to observed values. The fourth term is the degree of agreement and appears in both the numerator and denominator. It is computed as the square of the ratio of the mean anomaly between WRF60 and observations and the standard deviation of the anomalies.

(ii) Pooled paired t-test

To identify which areas in space contribute most to the AOD added-value, we compare daily mean AOD fields from WRF-Chem at different resolutions and MODIS. We perform a pooled paired t-test to evaluate the null hypothesis that those differences come from normal distributions with equal means and equal but unknown variances (the test statistic has a Student's t distribution with df = n + m – 2, and the sample standard deviation is the pooled standard deviation, where n and m are the two sample sizes). The test is conducted by climatological season (e.g. winter = DJF) since there are fewer than 20 valid AOD observations in most 60 km grid cells for each calendar month (Fig. 2). Given the large number of hypothesis tests performed (i.e. one for each 60 km grid cell), we adjust the p-values using the False Discovery Rate (FDR) approach (Benjamini and Hochberg, 1995). In this approach, p-values from the t-tests are ranked from low to high ($p_1, p_2, \ldots, p_m$), then the test with the highest rank, j, satisfying:

$$p_j \le \frac{j}{m}\alpha \quad \textbf{(6)}$$

is identified. Here all p-values satisfying Eq. 6 with α=0.1 are considered significant.

(iii) Accuracy and Hit Rate in identification of AOD extremes

For each month we identify grid cells in which the wavelength specific AOD exceeds the 75th percentile value computed from all grid cells and define that as an extreme. Thus grid cells with extreme AOD are independently determined for MODIS and WRF-Chem at different resolutions. The spatial coherence in identification of extremes in the fields is quantified using two metrics: the *Accuracy* and the *Hit Rate* (*HR*). The *Accuracy* indicates the overall spatial coherence and is computed as the number of grid cells co-identified as extreme and non-extreme between WRF-Chem and MODIS relative to the total number of cells with valid data. The *HR* weights only correct identification of extremes in MODIS by WRF-Chem.

3 ~~3~~ Results

3.1 ~~Quantifying the value added of increased~~Model performance as a function of spatial resolution

When WRF-Chem is applied at 60 km resolution the degree of association of the resulting spatial fields of mean monthly AOD at the three wavelengths with MODIS varies seasonally. Smallest RMSD and highest Spearman spatial correlations (ρ) with MODIS observations generally occur during months with highest mean AOD (i.e. during summer, Fig. 1 d-f and Fig. 3), and reach a maximum in August (ρ = 0.60, Table 2~~Table 2~~). However, while the patterns of relative AOD variability are well captured, the absolute magnitudes and spatial gradients of AOD during the summer are underestimated by WRF60 (Fig. 1 d-f and Fig. 3, Table S1). High spatial correlations (ρ > 0.40) are also observed in March, April and November (Table 2~~Table 2~~), when the ratio of spatial standard deviations is closer to 1 (Fig. 1 d-f, Table S1). Only a weak wavelength dependence is observed in the performance metrics as described on Taylor diagrams. The spatial variability is generally more negatively biased for AOD at 660 nm (Table S1), indicating that WRF60 simulations tend to produce larger diameter aerosols homogeneously distributed over the domain, whereas MODIS observations indicate more spatial variability.

The performance of WRF60 simulations relative to MODIS contrasts with analyses of WRF12 and WRF12-remap. WRF12 and WRF12-remap indicate highest spatial correlations with MODIS observations throughout the summer months (ρ = 0.5-0.7, Table 2~~Table 2~~), although the bias towards simulation of more coarse aerosols than are observed is consistent across the two simulations and with prior research (see details provided in (Crippa et al., 2016)). However, simulations at 12 km (WRF12) show positive ρ with MODIS for all λ in all calendar months, while mean monthly spatial fields of AOD from WRF60 show low and/or negative correlations with MODIS during May, June, September, October and December, indicating substantial differences in the degree of correspondence with MODIS AOD in the two simulations, and higher fidelity of the enhanced resolution runs (Tables 2 and S1).

Monthly mean spatial fields of AOD(λ) as simulated by WRF12 or WRF12-remap exhibit positive Spearman correlation coefficients (ρ) with MODIS observations for all calendar months and range from ~ 0.25 for WRF12-remap (0.20 for WRF12) during winter to ~ 0.70 and 0.64, respectively during summer (Table 2~~Table 2~~). Spearman's ρ are uniformly higher in WRF12-remap than WRF12 indicating a mismatch in space in the high-resolution simulation (i.e. that grid cells with high AOD are slightly displaced in the 12 km simulations possibly due to the presence of sub-grid scale aerosol plumes (Rissman et al., 2013)). Mean monthly fields of AOD (all λ) from both WRF12 and WRF12-remap exhibit lower ρ with MODIS in February-April and November than the 60 km runs (Table 2~~Table 2~~). These discrepancies appear to be driven by conditions in the south of the domain. For example, differences between WRF60/WRF12-remap vs. MODIS during all seasons are significant according to the paired t-test over Florida and along most of the southern coastlines (Fig. 2). This region of significant differences extends up to ~ 40°N during summer and fall, reflecting the stronger north-south gradient in AOD from MODIS and WRF12-remap that is not captured by WRF60 (see example for λ = 550 nm, Fig. 3). These enhancements in the latitudinal gradients from WRF12-remap are also manifest in the physical variables (particularly specific humidity as discussed further below).

The differences in the absolute values of mean monthly AOD deriving from differences in the resolution at which WRF-Chem was applied are of sufficient magnitude (a difference of up to 0.2 in regions with a mean AOD value of 0.4), particularly in the summer months (Fig. 4), to raise concerns. However, detailed investigation of the simulations settings and repetition of the 60 km simulation resulted in virtually identical results indicating no fault can be found in the analysis. Further, we note that the eastern-half of North America was also identified as a region of high discrepancy in global ESM (Myhre et al., 2013a).

To further investigate differences in the simulation output due to spatial discretization we computed Brier Skill Scores (BSS). In this analysis AOD for each λ from WRF12-remap are used as the ‘forecast’, output from WRF60 are used as the reference forecast and MODIS observations at 60 km are used as the target. BSS exceed 0 during all months except for September and October, and largest BSS (> 0.5) for AOD (all λ) is found during most months between December and July (Fig. 5a-c). This indicates that running WRF-Chem at 12 km resolution ~~adds value~~yields higher skill in simulated AOD relative to WRF60, even when the WRF12 output is remapped to 60 km. BSS do not strongly depend on λ, indicating the added value from enhanced resolution similarly affects aerosol particles of different sizes. Inspecting the terms defining the BSS provides information about the origin of the added value (Fig. 5a-c). The positive BSS derives principally from the potential skill (first term in Eq. 5), which demonstrates a reduction in bias and/or more accurate representation of the spatial gradients in WRF12-remap. This term exhibits weak seasonality with values below 0.5 only during August and fall months. The second and third terms are close to zero during most months, although bigger biases are found during August-October. The substantial conditional bias during late summer and early fall is the result of the large ratio of standard deviations (> 1, i.e. the spatial variability of the anomaly relative to MODIS is larger for WRF12-remap than WRF60, Table S1). It thus contributes to the negative BSS found in September and October, which are also identified as outlier months in WRF12-remap from the Taylor diagram analysis (Fig. 1). Output for these months show modest spatial correlations with AOD from MODIS and higher ratio of standard deviations than in WRF60-MODIS comparisons (Fig. 1, Table S1). Previous work showed that the lower model skill (in WRF12) during September and October may be partially attributable to a dry bias in precipitation from WRF-Chem relative to observations. As a result, simulated AOD and near-surface aerosol nitrate and sulfate concentrations are positively biased over large parts of the domain (Crippa et al., 2016). Although the effects of the boundary conditions appear in some variables (e.g. in Fig. 4 and Figs. S1-S3), the BSS results do not significantly change even when those cells are removed from the analysis.

When the BSS is used to assess the skill of each model relative to MODIS AOD climatological mean over the years 2000-2014, WRF12-remap is found to add value relative to the climatology (i.e. BSS >0) during summer months and Nov-Jan whereas BSS for WRF60 is positive from late Fall to early Spring (Fig. 5d). The fact that WRF-Chem does not always outperform the climatology is expected since the model is based on time invariant emissions and skill~~s~~ is~~are~~ assessed relative to a year selected to be representative of the AOD climatology. Mean seasonal AOD from MODIS retrievals over the study region during 2008 lie within ±0.2 standard deviations of the climatology (Crippa et al., 2016). Interestingly, BSS for most months (excluding September) are higher for the WRF60 simulations conducted using lateral boundary conditions from NAM12 than GFS.

Model resolution also affects the *Accuracy* and *Hit Rate* (*HR*) for identification of areas of extreme AOD (AOD>75th percentile). Highest coherence in the identification of extreme AOD in space identified in WRF12-remap (and WRF12) relative to MODIS is found during May-August (*HR* = 53-77%) vs. WRF60 (*HR* = 17-54%, Table 3). Conversely highest *HR* are found for WRF60 and MODIS during winter and early spring, and indeed exceed those for WRF12 and WRF12-remap (Table 3, e.g. Feb: *HR* = 0.78 for WRF60, and 0.67 and 0.68 for WRF12 and WRF12-remap, respectively). These differences are consistent with the observation that WRF12-remap overestimates the scales of AOD coherence and AOD magnitude during the cold season along coastlines and over much of the domain in April (Fig. 3).

The synthesis of these analyses is thus that the higher resolution simulation increases the overall spatial correlation, decreases overall bias in AOD close to the peak of the solar spectrum relative to MODIS observations and therefore the higher-resolution simulations better represent aerosol direct climate forcing. However, WRF12-remap exhibits little improvement over WRF60 in terms of reproducing the spatial variability of AOD in the visible wavelengths and further that WRF12-remap tends to be more strongly positively biased in terms of mean monthly AOD outside of the summer months (Fig. 2 and Fig. 3). Also the improvement in detection of areas of extreme AOD in the higher resolution simulations (WRF12-remap) is manifest only during the warm season.

3.2 Investigating ~~the origin of the added value and~~ sources of error in simulated AOD

As documented above, WRF-Chem applied at either 60 or 12 km resolution over eastern North America exhibits some skill in reproducing observed spatial fields of AOD and the occurrence of extreme AOD values. However, marked discrepancies both in space and time are found, and at least some of them show a significant dependence on model resolution. Thus, we investigated a range of physical conditions and gas phase concentrations known to be strongly determinant of aerosol dynamics in terms of the BSS as a function of model resolution and also in terms of the mean monthly spatial patterns.

WRF12 even when remapped to 60 km provides more accurate description of key meteorological variables such as specific humidity (Q) within the boundary layer, *PBLH*, surface temperature and precipitation (see Fig. 6, S1, S2 and S3) when compared to MERRA-2, as indicated by the positive BSS during almost all months (Fig. 7a). Good qualitative agreement is observed for the spatial patterns and absolute magnitude of T_{2m} in both WRF60 and WRF12-remap relative to MERRA-2 for all seasons (Fig. S1) leading to only modest magnitude of BSS (i.e. value added by the higher resolution simulations (Fig. 7a)). The aerosol size distribution and therefore wavelength specific AOD exhibits a strong sensitivity to Q (Santarpia et al., 2005) due to the presence of hygroscopic components in atmospheric aerosols and thus the role of water uptake in determining aerosol diameter, refractivity and extinction coefficient (Zieger et al., 2013). For example, the hygroscopic growth factor, which indicates the change of aerosol diameter due to water uptake, is ~ 1.4 for pure ammonium sulfate with dry diameter of 532 nm at relative humidity of 80%, thus biases in representation atmospheric humidity may lead to big errors in simulated aerosol size and AOD (Flores et al., 2012). Our previous analyses of the 12 km resolution simulations indicated overestimation of sulfate aerosols (a highly hygroscopic aerosol component, and one which in many chemical forms exhibits strong hysteresis (Martin et al., 2004)) relative to observed near-surface $PM_{2.5}$ concentrations during all seasons except for winter (Crippa et al., 2016), leading to the hypothesis that simulated AOD and discrepancies therein may exhibit a strong dependence on Q. Consistent with that postulate, Q_{PBL} from WRF12-remap exhibits a moist bias in cloud-free grid cells mostly during warm months, whereas WRF60 is characterized by a dry bias during all seasons (Fig. 6). Despite the positive bias, WRF12-remap better captures the seasonal spatial patterns of Q_{PBL} in MERRA-2, leading to positive BSS for this variable in all calendar months. Thus, there is added value by higher-resolution simulations in representation of one of the key parameters dictating aerosol particle growth and optical properties. Spatial patterns of differences in Q_{PBL} from WRF60 and WRF12-remap relative to MERRA-2 (Fig. 6) exhibit similarities to differences in AOD (Fig. 4). WRF60 is dry-biased relative to WRF12 particularly during the summer (and fall) and underestimates Q_{PBL} relative to MERRA-2 during all seasons over the southern states and over most of continental US during summer and fall. Conversely, WRF12-remap overestimates Q_{PBL} over most of continental US during summer and fall relative to MERRA-2.

PBLH is a key variable for dictating near-surface aerosol concentrations but is highly sensitive to the physical schemes applied, and biases appear to be domain and resolution dependent. However, this parameter is comparatively difficult to assess because differences in *PBLH* from WRF-Chem and MERRA-2 may also originate from the way they are computed (i.e. from heat diffusivity in MERRA-2 (Jordan et al., 2010) and from turbulent kinetic energy in WRF-Chem (Janjić, 2002;von Engeln and Teixeira, 2013)). Nevertheless, the Mellor-Yamada-Janjich *PBL* scheme combined with the Noah Land Surface Model applied in this work was found to produce lower *PBL* heights (Zhang et al., 2009) than other parameterizations. Thus, the positive bias in simulated AOD and surface $PM_{2.5}$ concentrations (reported previously in (Crippa et al., 2016)) may be linked to the systematic underestimation of *PBLH* simulated by WRF12-remap over continental US relative to MERRA-2 during all seasons (except winter) with greatest bias over regions of complex topography (Fig. S2). A positive bias (of several hundred meters) in terms of *PBLH* for WRF simulations using the MYJ parameterization was previously reported for high-resolution simulations over complex terrain (Rissman et al., 2013), and a positive bias in *PBLH* is also observed in the 60 km simulations presented herein (Fig. S2). This may provide a partial explanation for the ~~strong~~ large negative bias in AOD in WRF60 during summer (Fig. 3). In general, the BSS indicate improvement in the simulation of *PBLH* in WRF12-remap than in WRF60 (Fig. 7a).

Consistent with the dry bias in Q_{PBL} in WRF60, total accumulated precipitation is also underestimated in WRF60, while WRF12-remap captures the absolute magnitudes and the spatial patterns therein (Fig. S3). ~~Analysis~~ Analyses of hourly precipitation rates also show~~ed~~ higher skill ~~of~~ for WRF12-remap than WRF60 in ~~correctly~~ simulating precipitation occurrence (*HR*) relative to MERRA-2 (Table S2). More specifically WRF12-remap correctly predicts between 40% and 70 % of precipitation events in MERRA-2 with highest skill during winter months, whereas WRF60 output exhibits lower HR (~6% during summer and 30% during winter). This result thus confirms our expectation of a strong sensitivity of model performance to resolution due to the inherent scale dependence in the cumulus scheme. Use of the Grell-

Freitas parameterization in the WRF60 simulations did not lead to substantially different magnitude and/or spatial patterns of precipitation compared to WRF60 applied with the Grell 3D scheme, and no improvement in agreement with output from MERRA2. The findings of a negative bias in precipitation amounts in WRF60 simulations without a corresponding overestimation of AOD may appear counter-intuitive since aerosol concentrations (and thus AOD) are dependent on aerosol residence times and analyses of sixteen global models from the AeroCom project indicate wet scavenging is the dominant removal process for most aerosol species in the study area (Hand et al., 2012;Textor et al., 2006). However, the negative precipitation bias in WRF60 simulations appears to also be linked to poor representation of surface moisture availability, boundary layer humidity (Fig. 6), and ultimately aerosol water content (and hence AOD).

Gas phase concentrations (transformed into z-scores) from WRF12-remap show higher agreement with satellite observations during almost all months, as indicated by the positive BSS (Fig. 7b). However given the limited availability of valid satellite observations (especially during months with low radiation intensity), the BSS are likely only robust for the summer months for all species. Nevertheless, with the exception of NH_3 during June, BSS for all months are above or close to zero indicating that on average, the enhanced resolution simulations do ~~improve the quality~~exhibit higher skill in ~~of~~ the simulation of the gas phase species even when remapped to 60 km resolution. Further, the seasonal average spatial patterns of the total columnar concentrations, expressed in terms of z-scores, also exhibit qualitative agreement with the satellite observations (Fig. S4-S7).

4 Concluding remarks

This analysis is one of the first to quantify the impact of model spatial resolution on the spatio-temporal variability and magnitude of meteorological and chemical parameters and how representation of these variables impacts AOD, and does so using simulations for a full calendar year. Application of WRF-Chem at two different resolutions (60 km and 12 km) over eastern North America for a representative year (2008) leads to the following conclusions:

- Higher-resolution simulations ~~also add value in~~improve the representation of ~~other~~ key meteorological variables such as temperature, near-surface specific humidity, boundary layer height and the occurrence and amount of ~~precipitation~~precipitation. Both spatial patterns and precipitation occurrence are better captured by WRF12-remap, and particularly during the summer months the specific humidity within the boundary-layer exhibits closer agreement with a reanalysis product when WRF is applied at higher resolution. The dry bias in the low-resolution WRF-Chem simulations (60 km) is consistent with previous research over eastern North America, and is manifest in simulations with two different cumulus parameterizations and two different data sets for the LBC (GFS and NAM-12).

- More accurate representation of spatial patterns and ~~magnitude~~concentration of gaseous species that either play a key role in particle formation and growth or are indicators of primary aerosol emissions is also achieved by running WRF-Chem at high resolution.
- Partly/largely due to the improved fidelity of key meteorological parameters and gas-phase aerosol precursor species, h~~H~~igher resolution simulations enhance the fidelity of AOD representation at and near to the peak in the solar spectrum~~)~~ relative to a coarser run. ~~, although the improvement in model performance is not uniform in space and time. The higher skill of WRF12 and WRF12-remap appear to be linked to the improved representation of meteorological and chemical parameters.~~ At least some of the improvement in the accuracy with which AOD is reproduced in the higher resolution simulations may be due to improved fidelity of specific humidity and thus more accurate representation of hygroscopic growth of some aerosol components. Spatial correlations of AOD from WRF12 and WRF12-remap with observations from MODIS are higher than AOD from a simulation conducted at 60 km during most months. WRF12 show positive spatial correlations with MODIS for all λ in all calendar months, and particularly during summer (ρ = 0.5-0.7). However, the improvement in model performance is not uniform in space and time.
- ~~Spatial correlations of AOD from WRF12 and WRF12-remap with observations from MODIS are higher than AOD from a simulation conducted at 60 km during most months. WRF12 show positive spatial correlations with MODIS for all λ in all calendar months, and particularly during summer (ρ = 0.5-0.7).~~
- Output from WRF12 and WRF12-remap exhibit highest accord with MODIS observations in capturing the frequency, magnitude and location of extreme AOD values during summer when AOD is typically highest. During May-August WRF12-remap has *Hit Rates* for identification of extreme AOD of 53-78%.
- ~~At coarse resolution, WRF-Chem exhibits less sensitivity to the adopted lateral boundary conditions and cumulus scheme than to its spatial resolution.~~

~~Naturally, there is a need for more research regarding the sensitivity of WRF-Chem~~

~~simulations of climate relevant aerosol properties to the parameterizations used, the lateral boundary conditions employed and the resolution at which the simulations are conducted. Further, the contribution of the sole enhanced spatial resolution to the added value in AOD still needs to be quantified by identifying simulation settings that allow a bias reduction in all variables affecting AOD and will be part of future investigations.~~

- ~~Higher resolution simulations add value (i.e. enhance the fidelity of AOD at and near to the peak in the solar spectrum) relative to a coarser run, although the improvement in model performance is not uniform in space and time. Brier Skill Scores for the remapped simulations (i.e. output from simulations conducted at 12 km (WRF12) then averaged to 60 km, WRF12-remap) are positive for ten of twelve calendar moths, and for AOD(λ=550 nm) exceed 0.5 for seven of twelve months.~~
- ~~Spatial correlations of output from WRF12 and WRF12-remap with observations from MODIS are higher than output from a simulation conducted at 60 km during most months. For example, in contrast to WRF-Chem simulations at 60 km (WRF60), simulations conducted at 12 km (WRF12) show positive spatial correlations with MODIS for all λ in all calendar months, and particularly during summer (ρ = 0.5-0.7).~~
- ~~Output from WRF12 and WRF12-remap exhibit highest accord with MODIS observations in capturing the frequency, magnitude and location of extreme AOD values during summer when AOD is typically highest. During May-August WRF12-remap has *Hit Rates* for identification of extreme AOD of 53-78%.~~
- ~~Higher-resolution simulations also add value in the representation of other key meteorological variables such as temperature, boundary layer height and precipitation. Both spatial patterns and precipitation occurrence are better captured by WRF12-remap.~~
- ~~At least some of the improvement in the accuracy with which AOD is reproduced in the higher resolution simulations may be due to improved fidelity of specific humidity and thus more accurate representation of hygroscopic growth of some aerosol components.~~
- ~~More accurate representation of spatial patterns and magnitude of gaseous species that play a key role in particle formation and growth is also achieved by running WRF-Chem at high resolution.~~

It is worthy of note that even the 12 km resolution WRF-Chem simulations exhibit substantial differences in AOD relative to MODIS over eastern North America, and the agreement varies only slightly with wavelength. This may be partially attributable to use of the modal approach to represent the aerosol size distribution in order to enhance computational tractability. In this application each mode has a fixed geometric standard deviation (σ_g), which can lead to biases in simulated AOD in the visible wavelengths by up to 25% (Brock et al., 2016) (with the model overestimating observations if the prescribed σ_g is larger than the observed one). Setting σ_g = 2 for the accumulation mode (the default in WRF-Chem) may lead to an overestimation of the number of particles at the end of the accumulation mode tail, and there is evidence that a value of $\sigma_{g,acc}$=1.40 leads to higher agreement with observations (Mann et al., 2012). Further possible sources of the AOD biases reported herein derive from selection of the physical schemes (e.g. planetary boundary layer (*PBL*) schemes and land-surface model (Misenis and Zhang, 2010;Zhang et al., 2009)). Further, it is worth mentioning that NEI emissions are specified based on an average summertime weekday, so enhanced model performance might be achieved if seasonally varying emissions were available.

Naturally, there is a need for more research regarding the sensitivity of WRF-Chem simulations of climate relevant aerosol properties to the parameterizations used, the lateral boundary conditions employed and the resolution at which the simulations are conducted. –Further, attribution of added-value in the simulation of AOD by enhanced spatial resolution is necessary and will be facilitated by identifying simulation settings that minimize bias in the variables affecting AOD. This research will be part of future investigations.

~~Naturally, there is a need for more research regarding the sensitivity of WRF-Chem simulations of climate relevant aerosol properties to the parameterizations used, the lateral boundary conditions employed and the resolution at which the simulations are conducted.~~

Acknowledgments

This research was supported in part by a L'Oréal-UNESCO UK and Ireland Fellowship For Women In Science (to PC), the Natural Environmental Research Council (NERC) through the LICS project (ref. NE/K010794/1), grants to SCP from US NSF (grant # 1517365) and NASA (NNX16AG31G), and a NASA Earth and Space Science Fellowship Program - Grant "14-EARTH14F-0207" (to RCS). Further support was provided by the Lilly Endowment, Inc., through its support for the Indiana University Pervasive Technology Institute and the Indiana METACyt Initiative. We gratefully acknowledge the NASA scientists responsible for

MERRA-2 and MODIS products, the developers of WRF-Chem, and Lieven Clarisse, Simon Whitburn, and Martin Van Damme for producing and sharing the NH_3 retrievals. The clarity and content of this manuscript was substantially improved by the comments of three reviewers.

References

Ackermann, I. J., Hass, H., Memmesheimer, M., Ebel, A., Binkowski, F. S., and Shankar, U.: Modal aerosol dynamics model for Europe: development and first applications, Atmospheric Environment, 32, 2981-2999, http://dx.doi.org/10.1016/S1352-2310(98)00006-5, 1998.

Anderson, T. L., Charlson, R. J., Winker, D. M., Ogren, J. A., and Holmén, K.: Mesoscale Variations of Tropospheric Aerosols, Journal of the Atmospheric Sciences, 60, 119-136, doi: http://dx.doi.org/10.1175/1520-0469(2003)060<0119:MVOTA>2.0.CO;2, 2003.

Ångström, A.: The parameters of atmospheric turbidity, Tellus, 16, 64-75, 10.1111/j.2153-3490.1964.tb00144.x, 1964.

Arakawa, A.: The Cumulus Parameterization Problem: Past, Present, and Future, Journal of Climate, 17, 2493-2525, doi:10.1175/1520-0442(2004)017<2493:RATCPP>2.0.CO;2, 2004.

Benjamini, Y., and Hochberg, Y.: Controlling the False Discovery Rate: A Practical and Powerful Approach to Multiple Testing, Journal of the Royal Statistical Society. Series B (Methodological), 57, 289-300, 1995.

Boucher, O., D. Randall, P. Artaxo, C. Bretherton, G. Feingold, P. Forster, V.-M. Kerminen, Y. Kondo, H. Liao, U. Lohmann, P. Rasch, S.K. Satheesh, S. Sherwood, B. Stevens and X.Y. Zhang: Clouds and Aerosols, in: Climate Change 2013: The Physical Science Basis. Contribution of Working Group I to the Fifth Assessment Report of the Intergovernmental Panel on Climate Change, edited by: Stocker, T. F., D. Qin, G.-K. Plattner, M. Tignor, S.K. Allen, J. Boschung, A. Nauels, Y. Xia, V. Bex and P.M. Midgley, Cambridge University Press, Cambridge, United Kingdom and New York, NY, USA, 33–115, 2013.

Brinksma, E. J., Boersma, K. F., Levelt, P. F., and McPeters, R. D.: OMI validation requirements document, Version 1, Rep. RS-OMIE-KNMI-345, 66, 2003.

Brock, C. A., Wagner, N. L., Anderson, B. E., Attwood, A. R., Beyersdorf, A., Campuzano-Jost, P., Carlton, A. G., Day, D. A., Diskin, G. S., Gordon, T. D., Jimenez, J. L., Lack, D. A., Liao, J., Markovic, M. Z., Middlebrook, A. M., Ng, N. L., Perring, A. E., Richardson, M. S., Schwarz, J. P., Washenfelder, R. A., Welti, A., Xu, L., Ziemba, L. D., and Murphy, D. M.: Aerosol optical properties in the southeastern United States in summer – Part 1: Hygroscopic growth, Atmospheric Chemistry and Physics, 16, 25695-25738, doi:10.5194/acp-16-5009-2016, 2016.

Chance, K.: OMI algorithm theoretical basis document, volume IV: OMI trace gas algorithms, 2002.

Chen, F., and Dudhia, J.: Coupling an advanced land surface–hydrology model with the Penn State–NCAR MM5 modeling system. Part I: model implementation and sensitivity, Monthly Weather Review, 129, 569-585, doi:10.1175/1520-0493(2001)129<0569:CAALSH>2.0.CO;2, 2001.

Chin, M., Kahn, R. A., and Schwartz , S. E.: Atmospheric Aerosols Properties and Climate Impacts. A Report by the U.S. Climate Change Science Program and the Subcommittee on Global Change Research, in, National Aeronautics and Space Administration, Washington, D.C., USA, 128, 2009.

Crippa, P., Sullivan, R. C., Thota, A., and Pryor, S. C.: Evaluating the skill of high-resolution WRF-Chem simulations in describing drivers of aerosol direct climate forcing on the regional scale, Atmospheric Chemistry and Physics, 16, 397-416, 10.5194/acp-16-397-2016, 2016.

Di Luca, A., de Elía, R., and Laprise, R.: Challenges in the Quest for Added Value of Regional Climate Dynamical Downscaling, Curr Clim Change Rep, 1, 10-21, 10.1007/s40641-015-0003-9, 2015.

Diaconescu, E., and Laprise, R.: Can added value be expected in RCM-simulated large scales?, Climate Dynamics, 41, 1769-1800, 10.1007/s00382-012-1649-9, 2013.

Emmons, L. K., Walters, S., Hess, P. G., Lamarque, J. F., Pfister, G. G., Fillmore, D., Granier, C., Guenther, A., Kinnison, D., Laepple, T., Orlando, J., Tie, X., Tyndall, G., Wiedinmyer, C., Baughcum, S. L., and Kloster, S.: Description and evaluation of the Model for Ozone and Related chemical Tracers, version 4 (MOZART-4), Geoscientific Model Development, 3, 43-67, doi:10.5194/gmd-3-43-2010, 2010.

Fast, J. D., Gustafson, W. I., Easter, R. C., Zaveri, R. A., Barnard, J. C., Chapman, E. G., Grell, G. A., and Peckham, S. E.: Evolution of ozone, particulates, and aerosol direct radiative forcing in the vicinity of Houston using a fully coupled meteorology-chemistry-aerosol model, Journal of Geophysical Research: Atmospheres, 111, D21305, 10.1029/2005JD006721, 2006.

Fioletov, V. E., McLinden, C. A., Krotkov, N., Moran, M. D., and Yang, K.: Estimation of SO_2 emissions using OMI retrievals, Geophysical Research Letters, 38, L21811, 10.1029/2011GL049402, 2011.

Flores, J. M., Bar-Or, R. Z., Bluvshtein, N., Abo-Riziq, A., Kostinski, A., Borrmann, S., Koren, I., Koren, I., and Rudich, Y.: Absorbing aerosols at high relative humidity: linking hygroscopic growth to optical properties, Atmospheric Chemistry and Physics, 12, 5511-5521, 10.5194/acp-12-5511-2012, 2012.

Grell, G. A., and Dévényi, D.: A generalized approach to parameterizing convection combining ensemble and data assimilation techniques, Geophysical Research Letters, 29, 38-31-38-34, 10.1029/2002GL015311, 2002.

Grell, G. A., Peckham, S. E., Schmitz, R., McKeen, S. A., Frost, G., Skamarock, W. C., and Eder, B.: Fully coupled "online" chemistry within the WRF model, Atmospheric Environment, 39, 6957-6975, 10.1016/j.atmosenv.2005.04.027, 2005.

Grell, G. A., and Freitas, S. R.: A scale and aerosol aware stochastic convective parameterization for weather and air quality modeling, Atmospheric Chemistry and Physics, 14, 5233-5250, 10.5194/acp-14-5233-2014, 2014.

Guenther, A., Zimmerman, P., and Wildermuth, M.: Natural volatile organic compound emission rate estimates for U.S. woodland landscapes, Atmospheric Environment, 28, 1197-1210, 10.1016/1352-2310(94)90297-6, 1994.

Guenther, A. B., Zimmerman, P. R., Harley, P. C., Monson, R. K., and Fall, R.: Isoprene and monoterpene emission rate variability: model evaluations and sensitivity analyses, J. Geophys. Res.-Atmos., 98, 12609-12617, 10.1029/93jd00527, 1993.

Gustafson, W. I., Qian, Y., and Fast, J. D.: Downscaling aerosols and the impact of neglected subgrid processes on direct aerosol radiative forcing for a representative global climate model grid spacing, Journal of Geophysical Research: Atmospheres, 116, D13303, 10.1029/2010JD015480, 2011.

Hand, J. L., Schichtel, B. A., Pitchford, M., Malm, W. C., and Frank, N. H.: Seasonal composition of remote and urban fine particulate matter in the United States, J. Geophys. Res.-Atmos., 117, 10.1029/2011jd017122, 2012.

Hong, S.-Y., Dudhia, J., and Chen, S.-H.: A Revised Approach to Ice Microphysical Processes for the Bulk Parameterization of Clouds and Precipitation, Monthly Weather Review, 132, 103-120, doi:10.1175/1520-0493(2004)132<0103:ARATIM>2.0.CO;2, 2004.

Hyer, E. J., Reid, J. S., and Zhang, J.: An over-land aerosol optical depth data set for data assimilation by filtering, correction, and aggregation of MODIS Collection 5 optical depth retrievals, Atmospheric Measurement Techniques, 4, 379-408, 10.5194/amt-4-379-2011, 2011.

Janjić, Z. I.: The Step-Mountain Eta Coordinate Model: Further Developments of the Convection, Viscous Sublayer, and Turbulence Closure Schemes, Monthly Weather Review, 122, 927-945, doi:10.1175/1520-0493(1994)122<0927:TSMECM>2.0.CO;2, 1994.

Janjić, Z. I.: Nonsingular implementation of the Mellor–Yamada level 2.5 scheme in the NCEP Meso model, NCEP office note, 437, 61, 2002.

Jankov, I., A. Gallus, J. W., Segal, M., Shaw, B., and E. Koch, S.: The Impact of Different WRF Model Physical Parameterizations and Their Interactions on Warm Season MCS Rainfall, Weather and Forecasting, 20, 1048-1060, doi:10.1175/WAF888.1, 2005.

Jordan, N. S., Hoff, R. M., and Bacmeister, J. T.: Validation of Goddard Earth Observing System-version 5 MERRA planetary boundary layer heights using CALIPSO, J. Geophys. Res.-Atmos., 115, 10.1029/2009jd013777, 2010.

Krotkov, N. A., McClure, B., Dickerson, R. R., Carn, S. A., Li, C., Bhartia, P. K., Yang, K., Krueger, A. J., Li, Z., Levelt, P. F., Chen, H., Wang, P., and Lu, D.: Validation of SO_2 retrievals from the Ozone Monitoring Instrument over NE China, Journal of Geophysical Research: Atmospheres, 113, D16S40, 10.1029/2007JD008818, 2008.

Leibensperger, E., Mickley, L. J., Jacob, D. J., Chen, W.-T., Seinfeld, J., Nenes, A., Adams, P., Streets, D., Kumar, N., and Rind, D.: Climatic effects of 1950–2050 changes in US anthropogenic aerosols–Part 1: Aerosol trends and radiative forcing, Atmospheric Chemistry and Physics, 12, 3333-3348, doi:10.5194/acp-12-3333-2012, 2012.

Levy, R. C., Mattoo, S., Munchak, L. A., Remer, L. A., Sayer, A. M., Patadia, F., and Hsu, N. C.: The Collection 6 MODIS aerosol products over land and ocean, Atmospheric Measurement Techniques, 6, 2989-3034, 10.5194/amt-6-2989-2013, 2013.

Li, L. F., Li, W. H., and Jin, J. M.: Improvements in WRF simulation skills of southeastern United States summer rainfall: physical parameterization and horizontal resolution, Climate Dynamics, 43, 2077-2091, 10.1007/s00382-013-2031-2, 2014.

Long, M., Yantosca, R., Nielsen, J., Keller, C., da Silva, A., Sulprizio, M., Pawson, S., and Jacob, D.: Development of a grid-independent GEOS-Chem chemical transport model (v9-02) as an atmospheric chemistry module for Earth system models, Geoscientific Model Development, 8, 595-602, doi:10.5194/gmd-8-595-2015, 2015.

Lowrey, M. R. K., and Yang, Z. L.: Assessing the Capability of a Regional-Scale Weather Model to Simulate Extreme Precipitation Patterns and Flooding in Central Texas, Weather and Forecasting, 23, 1102-1126, 10.1175/2008waf2006082.1, 2008.

Mann, G. W., Carslaw, K. S., Ridley, D. A., Spracklen, D. V., Pringle, K. J., Merikanto, J., Korhonen, H., Schwarz, J. P., Lee, L. A., Manktelow, P. T., Woodhouse, M. T., Schmidt, A., Breider, T. J., Emmerson, K. M., Reddington, C. L., Chipperfield, M. P., and Pickering, S. J.: Intercomparison of modal and sectional aerosol microphysics representations within the same 3-D global chemical transport model, Atmospheric Chemistry and Physics, 12, 4449-4476, 10.5194/acp-12-4449-2012, 2012.

Martin, S. T., Hung, H. M., Park, R. J., Jacob, D. J., Spurr, R. J. D., Chance, K. V., and Chin, M.: Effects of the physical state of tropospheric ammonium-sulfate-nitrate particles on global aerosol direct radiative forcing, Atmospheric Chemistry and Physics, 4, 183-214, doi:10.5194/acp-4-183-2004, 2004.

McComiskey, A., Schwartz, S. E., Schmid, B., Guan, H., Lewis, E. R., Ricchiazzi, P., and Ogren, J. A.: Direct aerosol forcing: Calculation from observables and sensitivities to inputs, Journal of Geophysical Research: Atmospheres, 113, D09202, 10.1029/2007JD009170, 2008.

McLinden, C. A., Fioletov, V., Boersma, K. F., Kharol, S. K., Krotkov, N., Lamsal, L., Makar, P. A., Martin, R. V., Veefkind, J. P., and Yang, K.: Improved satellite retrievals of NO_2 and SO_2 over the Canadian oil sands and comparisons with surface measurements, Atmospheric Chemistry and Physics, 14, 3637-3656, 10.5194/acp-14-3637-2014, 2014.

Mearns, L. O., Arritt, R., Biner, S., Bukovsky, M., Stain, S., and NARCCAP team The North American Regional Climate Change Assessment Program: Overview of Phase I Results, Bulletin of the American Meteorological Society, 93, 1337-1362, 2012.

Meehl, G. A., Moss, R., Taylor, K. A., Eyring, V., Stouffer, R. J., Sandrine, B., and Stevens, B.: Climate model intercomparisons: preparing for the next phase, Eos, Transaction, American Geophysical Union, 95, 77-84, doi:10.1002/2014EO09, 2014.

Misenis, C., and Zhang, Y.: An examination of sensitivity of WRF/Chem predictions to physical parameterizations, horizontal grid spacing, and nesting options, Atmospheric Research, 97, 315-334, 10.1016/j.atmosres.2010.04.005, 2010.

Mlawer, E. J., Taubman, S. J., Brown, P. D., Iacono, M. J., and Clough, S. A.: Radiative transfer for inhomogeneous atmospheres: RRTM, a validated correlated-k model for the longwave, Journal of Geophysical Research: Atmospheres, 102, 16663-16682, 10.1029/97JD00237, 1997.

Molod, A., Takacs, L., Suarez, M., and Bacmeister, J.: Development of the GEOS-5 atmospheric general circulation model: evolution from MERRA to MERRA2, Geoscientific Model Development, 8, 1339-1356, 10.5194/gmd-8-1339-2015, 2015.

Murphy, A. H., and Epstein, E. S.: Skill scores and correlation-coefficients in model verification, Monthly Weather Review, 117, 572-581, 10.1175/1520-0493(1989)117<0572:ssacci>2.0.co;2, 1989.

Myhre, G., Samset, B. H., Schulz, M., Balkanski, Y., Bauer, S., Berntsen, T. K., Bian, H., Bellouin, N., Chin, M., Diehl, T., Easter, R. C., Feichter, J., Ghan, S. J., Hauglustaine, D., Iversen, T., Kinne, S., Kirkevag, A., Lamarque, J. F., Lin, G., Liu, X., Lund, M. T., Luo, G., Ma, X., van Noije, T., Penner, J. E., Rasch, P. J., Ruiz, A., Seland, O., Skeie, R. B., Stier, P., Takemura, T., Tsigaridis, K., Wang, P., Wang, Z., Xu, L., Yu, H., Yu, F., Yoon, J. H., Zhang, K., Zhang, H., and Zhou, C.: Radiative forcing of the direct aerosol effect from AeroCom Phase II simulations, Atmospheric Chemistry and Physics, 13, 1853-1877, 10.5194/acp-13-1853-2013, 2013a.

Myhre, G., Shindell, D., Bréon, F.-M., Collins, W., Fuglestvedt, J., Huang, J., Koch, D., Lamarque, J.-F., Lee, D., Mendoza, B., Nakajima, T., Robock, A., Stephens, G., Takemura, T., and Zhang, H.: Anthropogenic and Natural Radiative Forcing, in: Climate Change 2013: The Physical Science Basis. Contribution of Working Group I to the Fifth Assessment Report of the Intergovernmental Panel on Climate Change, edited by: Stocker, T. F., Qin, D., Plattner, G.-K., Tignor, M., Allen, S. K., Boschung, J., Nauels, A., Xia, Y., Bex, V., and Midgley, P. M., Cambridge University Press, Cambridge, United Kingdom and New York, NY, USA, 659–740, 2013b.

Nasrollahi, N., AghaKouchak, A., Li, J. L., Gao, X. G., Hsu, K. L., and Sorooshian, S.: Assessing the Impacts of Different WRF Precipitation Physics in Hurricane Simulations, Weather and Forecasting, 27, 1003-1016, 10.1175/waf-d-10-05000.1, 2012.

Qian, Y., Gustafson Jr, W. I., and Fast, J. D.: An investigation of the sub-grid variability of trace gases and aerosols for global climate modeling, Atmospheric Chemistry and Physics, 10, 6917-6946, 10.5194/acp-10-6917-2010, 2010.

Rissman, J., Arunachalam, S., Woody, M., West, J. J., BenDor, T., and Binkowski, F. S.: A plume-in-grid approach to characterize air quality impacts of aircraft emissions at the Hartsfield–Jackson Atlanta International Airport, Atmospheric Chemistry and Physics, 13, 9285-9302, 10.5194/acp-13-9285-2013, 2013.

Rockel, B., Castro, C. L., Pielke, R. A., von Storch, H., and Leoncini, G.: Dynamical downscaling: Assessment of model system dependent retained and added variability for two different regional climate models, Journal of Geophysical Research: Atmospheres, 113, D21107, 10.1029/2007JD009461, 2008.

Santarpia, J. L., Gasparini, R., Li, R. J., and Collins, D. R.: Diurnal variations in the hygroscopic growth cycles of ambient aerosol populations, J. Geophys. Res.-Atmos., 110, 10.1029/2004jd005279, 2005.

Schell, B., Ackermann, I. J., Hass, H., Binkowski, F. S., and Ebel, A.: Modeling the formation of secondary organic aerosol within a comprehensive air quality model system, J. Geophys. Res.-Atmos., 106, 28275-28293, 10.1029/2001jd000384, 2001.

Schuster, G. L., Dubovik, O., and Holben, B. N.: Angstrom exponent and bimodal aerosol size distributions, J. Geophys. Res.-Atmos., 111, D07207, doi:10.1029/2005JD006328., 2006.

Seinfeld, J. H., and Pandis, S. N.: Atmospheric chemistry and physics: from air pollution to climate change, John Wiley & Sons, 1152 pp., 2016.

Simes, R. J.: An improved Bonferroni procedure for multiple tests of significance, Biometrika, 73, 751-754, 10.2307/2336545, 1986.

Simpson, D., Guenther, A., Hewitt, C. N., and Steinbrecher, R.: Biogenic emissions in Europe. 1. estimates and uncertainties, J. Geophys. Res.-Atmos., 100, 22875-22890, 10.1029/95jd02368, 1995.

Stocker, T. F. a. Q., D. and Plattner, G.-K. and Alexander, L.V. and Allen, S.K. and Bindoff, N.L. and Bréon, F.-M. and Church, J.A. and Cubasch, U. and Emori, S. and Forster, P. and Friedlingstein, P. and Gillett, N. and Gregory, J.M. and Hartmann, D.L. and Jansen, E. and Kirtman, B. and Knutti, R. and Krishna Kumar, K. and Lemke, P. and Marotzke, J. and Masson-Delmotte, V. and Meehl, G.A. and Mokhov, I.I. and Piao, S. and Ramaswamy, V. and Randall, D. and Rhein, M. and Rojas, M. and Sabine, C. and Shindell, D. and Talley, L.D. and Vaughan, D.G. and Xie, S.-P.: Summary for Policymakers, in: Climate Change 2013: The Physical Science Basis. Contribution of Working Group I to the Fifth Assessment Report of the Intergovernmental Panel on Climate Change, Cambridge University Press, Cambridge, United Kingdom and New York, NY, USA, 33–115, 2013.

Stockwell, W. R., Middleton, P., Chang, J. S., and Tang, X.: The second generation regional acid deposition model chemical mechanism for regional air quality modeling, Journal of Geophysical Research: Atmospheres, 95, 16343-16367, 10.1029/JD095iD10p16343, 1990.

Sun, Y., Yi, L., Zhong, Z., and Ha, Y.: Performance of a New Convective Parameterization Scheme on Model Convergence in Simulations of a Tropical Cyclone at Grey-Zone Resolutions, Journal of the Atmospheric Sciences, 71, 2078-2088, doi:10.1175/JAS-D-13-0285.1, 2014.

Taylor, K. E.: Summarizing multiple aspects of model performance in a single diagram, J. Geophys. Res.-Atmos., 106, 7183-7192, 10.1029/2000jd900719, 2001.

Textor, C., Schulz, M., Guibert, S., Kinne, S., Balkanski, Y., Bauer, S., Berntsen, T., Berglen, T., Boucher, O., Chin, M., Dentener, F., Diehl, T., Easter, R., Feichter, H., Fillmore, D., Ghan, S., Ginoux, P., Gong, S., Kristjansson, J. E., Krol, M., Lauer, A., Lamarque, J. F., Liu, X., Montanaro, V., Myhre, G., Penner, J., Pitari, G., Reddy, S., Seland, O., Stier, P., Takemura, T., and Tie, X.: Analysis and quantification of the diversities of aerosol life cycles within AeroCom, Atmospheric Chemistry and Physics, 6, 1777-1813, 2006.

Tilmes, S., Lamarque, J.-F., Emmons, L., Kinnison, D., Ma, P.-L., Liu, X., Ghan, S., Bardeen, C., Arnold, S., and Deeter, M.: Description and evaluation of tropospheric chemistry and aerosols in the Community Earth System Model (CESM1. 2), Geoscientific Model Development, 8, 1395-1426, doi:10.5194/gmd-8-1395-2015, 2015.

Tomasi, C., Caroli, E., and Vitale, V.: Study of the Relationship between Ångström's Wavelength Exponent and Junge Particle Size Distribution Exponent, Journal of Climate and

Applied Meteorology, 22, 1707-1716, 10.1175/1520-0450(1983)022<1707:SOTRBW>2.0.CO;2, 1983.

US-EPA: 2005 National Emissions Inventory (NEI), US Environmental Protection Agency in, available at: ftp://aftp.fsl.noaa.gov/divisions/taq/emissions_data_2005/, 2009.

Vinken, G. C. M., Boersma, K. F., van Donkelaar, A., and Zhang, L.: Constraints on ship NO_x emissions in Europe using GEOS-Chem and OMI satellite NO_2 observations, Atmospheric Chemistry and Physics, 14, 1353-1369, 10.5194/acp-14-1353-2014, 2014.

von Engeln, A., and Teixeira, J.: A Planetary Boundary Layer Height Climatology Derived from ECMWF Reanalysis Data, Journal of Climate, 26, 6575–6590, doi: 10.1175/JCLI-D-12-00385.1, 2013.

Weigum, N., Schutgens, N., and Stier, P.: Effect of aerosol subgrid variability on aerosol optical depth and cloud condensation nuclei: implications for global aerosol modelling, Atmospheric Chemistry and Physics, 16, 13619-13639, 10.5194/acp-16-13619-2016, 2016.

Whitburn, S., Van Damme, M., Clarisse, L., Bauduin, S., Heald, C., Hadji-Lazaro, J., Hurtmans, D., Zondlo, M. A., Clerbaux, C., and Coheur, P.-F.: A flexible and robust neural network IASI-NH_3 retrieval algorithm, J. Geophys. Res.-Atmos., In Press, 10.1002/2016JD024828, 2016.

Wild, O., Zhu, X., and Prather, M. J.: Fast-J: Accurate Simulation of In- and Below-Cloud Photolysis in Tropospheric Chemical Models, Journal of Atmospheric Chemistry, 37, 245-282, 10.1023/a:1006415919030, 2000.

Zhang, X., Chen, Z. M., Wang, H. L., He, S. Z., and Huang, D. M.: An important pathway for ozonolysis of alpha-pinene and beta-pinene in aqueous phase and its atmospheric implications, Atmospheric Environment, 43, 4465-4471, 10.1016/j.atmosenv.2009.06.028, 2009.

Zhang, Y., He, J., Zhu, S., and Gantt, B.: Sensitivity of simulated chemical concentrations and aerosol-meteorology interactions to aerosol treatments and biogenic organic emissions in WRF/Chem, Journal of Geophysical Research: Atmospheres, 121, 6014-6048, 10.1002/2016JD024882, 2016.

Zieger, P., Fierz-Schmidhauser, R., Weingartner, E., and Baltensperger, U.: Effects of relative humidity on aerosol light scattering: results from different European sites, Atmospheric Chemistry and Physics, 13, 10609-10631, 10.5194/acp-13-10609-2013, 2013.

Figures

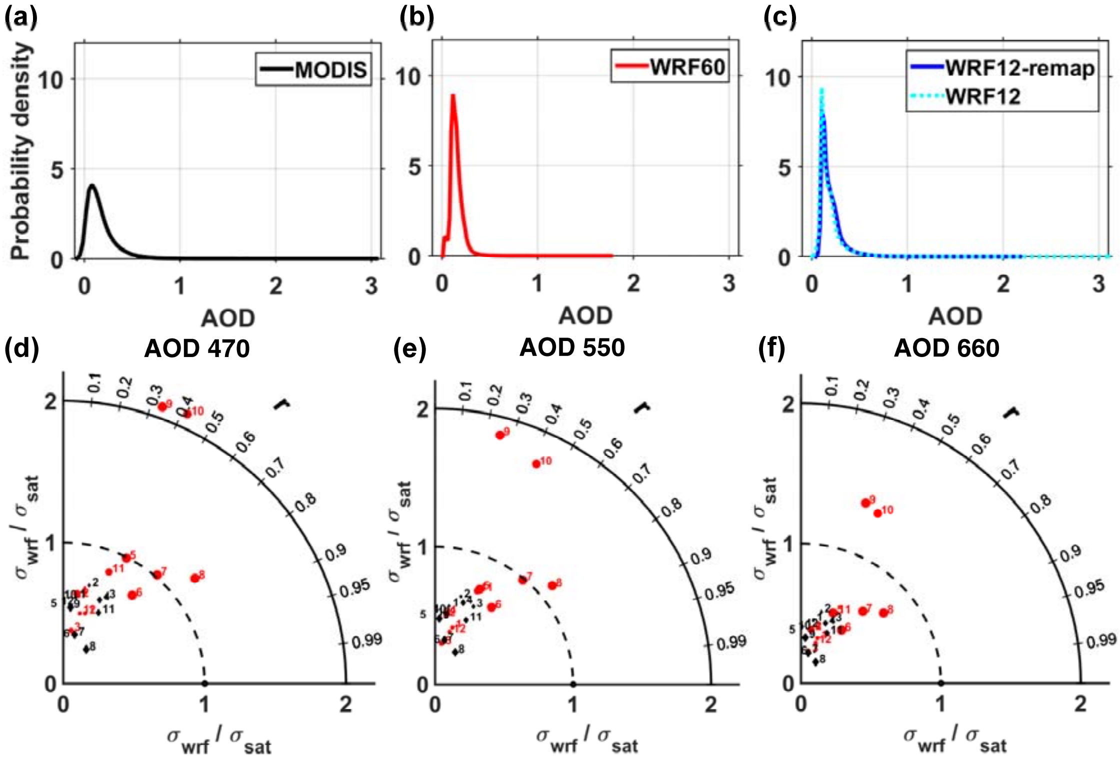

Figure 1. Probability density function of once daily AOD at a wavelength (λ) of 550 nm for (a) MODIS, (b) WRF60 and (c) WRF12 and WRF12-remap during the year 2008. (d-f) Taylor diagrams of mean monthly AOD at wavelengths (λ) of (d) 470, (e) 550 and (f) 660 nm as simulated by WRF-Chem at different resolutions (black diamonds=WRF60 and red dots=WRF12-remap) relative to MODIS observations. The numbers by each symbol denote the calendar month (e.g. 1=January).

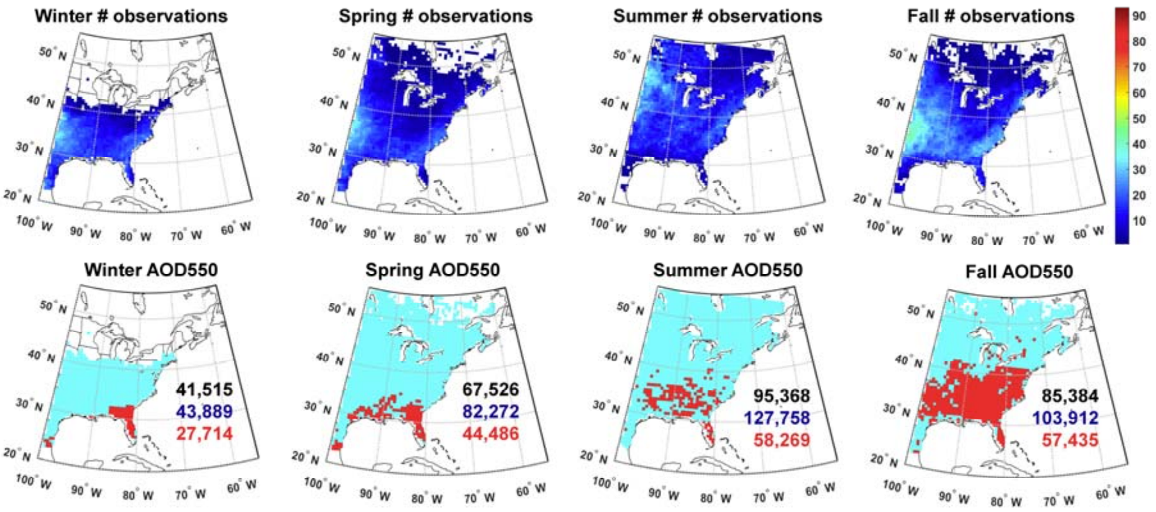

Figure 2. First line: Number of paired AOD observations at a wavelength (λ) of 550 nm (i.e. simultaneous values as output from WRF-Chem and observed by MODIS) used to perform a t-test designed to evaluate whether the difference computed for each grid cell as WRF60-MODIS differs from that computed as WRF12-remap-MODIS on a seasonal basis (columns show Winter (DJF), Spring (MAM), Summer (JJA) and Fall (SON)). Second line: Results of the t-test. Pixels that have p-values that are significantly different at α=0.10 are indicated in red and have been corrected for multiple testing using a False Discovery Rate approach. The number of observations of cloud-free conditions summed across all days in each season and all grid cells is also reported (black=MODIS, blue=WRF60, red=WRF12-remap).

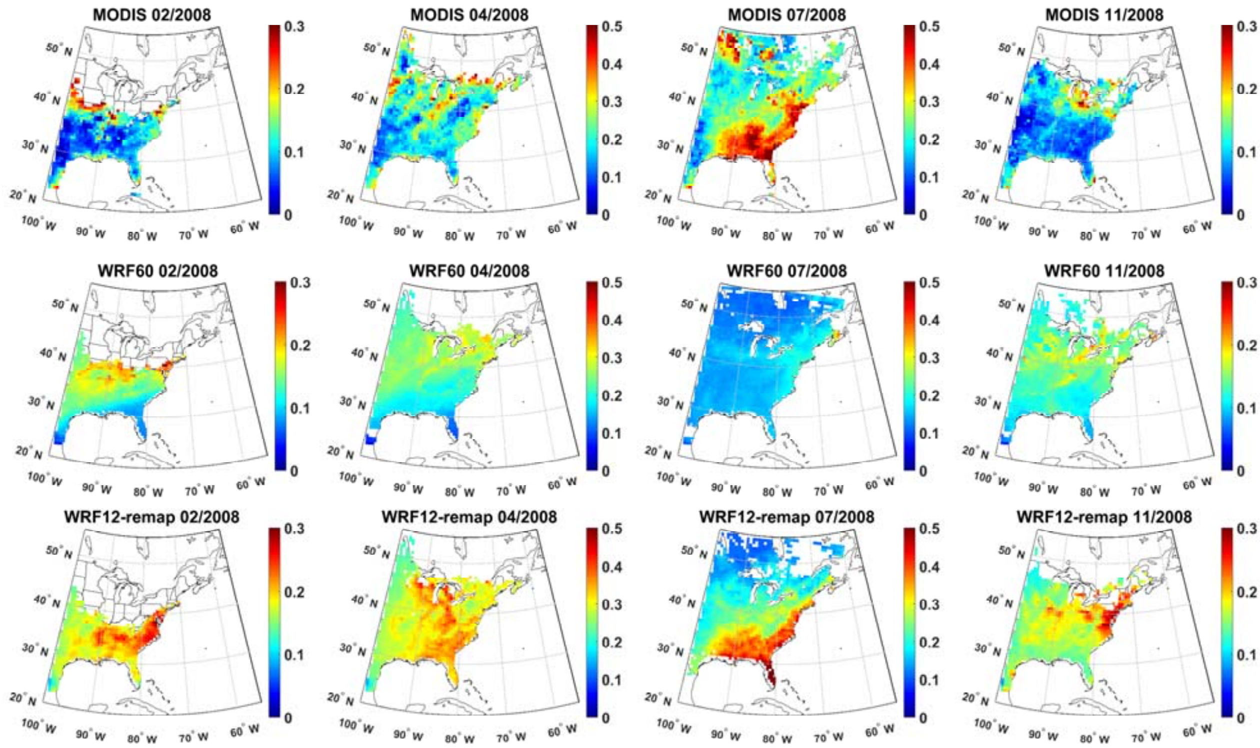

Figure 3. Monthly mean AOD at a wavelength (λ) of 550 nm from MODIS (first line) and WRF-Chem at different resolutions (WRF60 and WRF12-remap, second and third line) during a representative month in each climatological season (columns). Note that a different color scale is applied for different months. For a monthly mean value for a grid cell to be shown, there must be at least 5-simultaneous daily values (for the time of the satellite overpass) available.

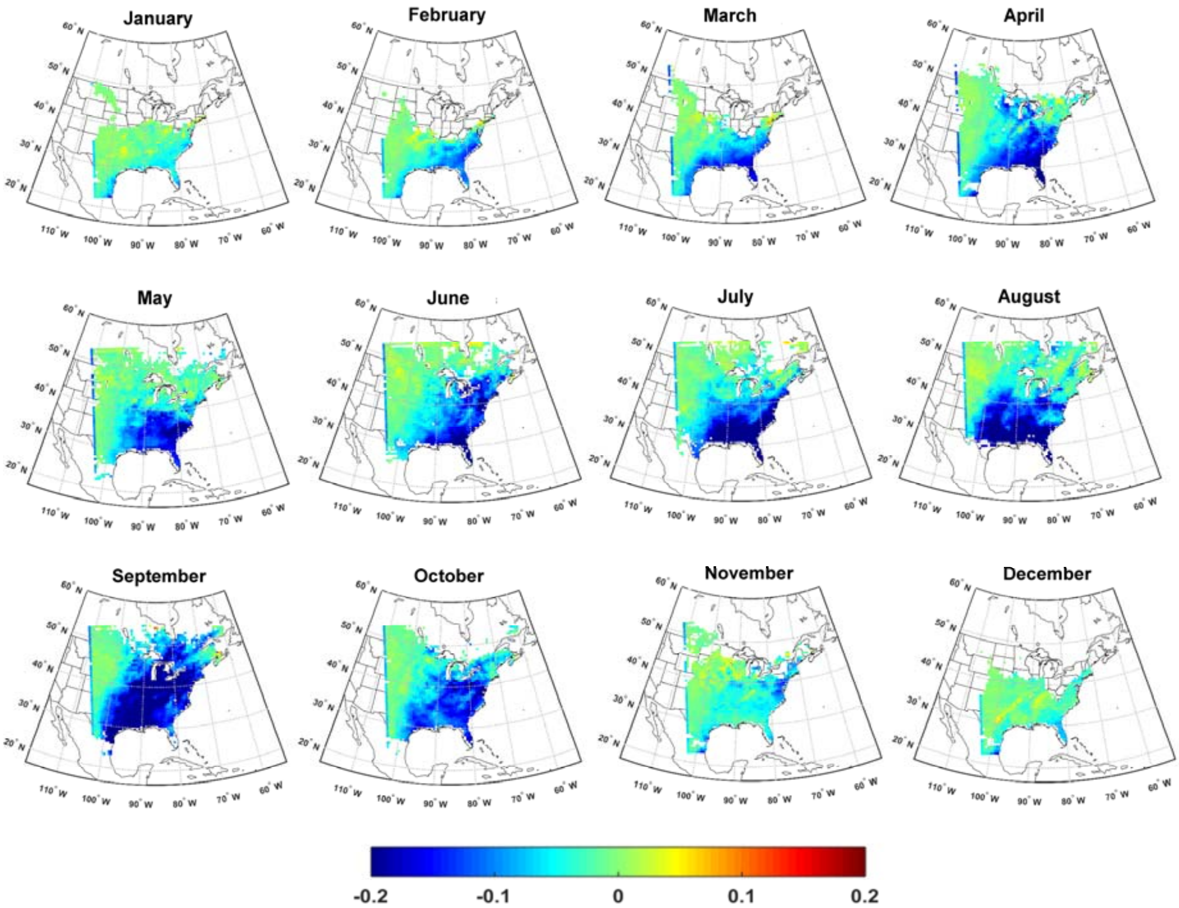

Figure 4. Difference in monthly mean AOD at a wavelength (λ) of 550 nm between WRF-Chem simulations conducted at 60 km resolution (WRF60) and output from WRF-Chem simulations conducted with a resolution of 12 km but remapped to 60 km (WRF12-remap). Differences are computed as WRF60 minus WRF12-remap. Similar spatial patterns and magnitudes of differences are found for λ of 470 and 660 nm. The calendar months of 2008 are shown in the titles of each panel.

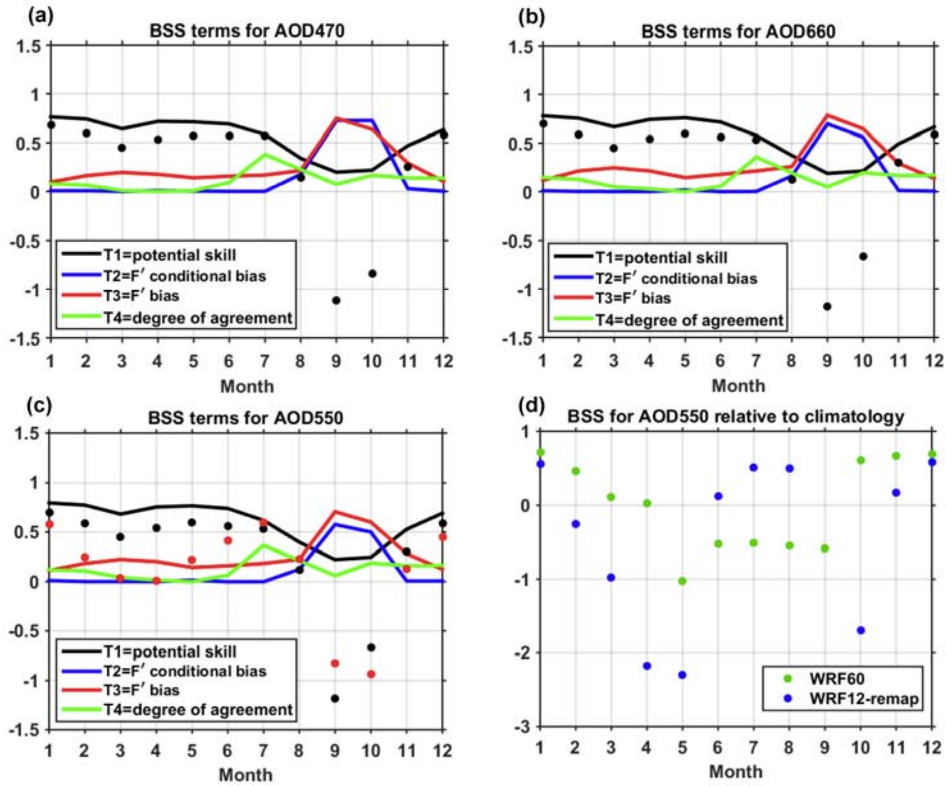

Figure 5. (a-c) Brier Skill Scores (BSS, black dots) for monthly mean AOD by calendar month (1=January) for AOD at 470, 550 and 660 nm. In this analysis of model skill WRF12 output is mapped to the WRF60 grid (WRF12-remap) and BSS are computed using MODIS as the target, WRF60 (driven by NAM12 meteorological boundary conditions) as the reference forecast and WRF12-remap as the forecast. Also shown by the color lines are the contributions of different terms to BSS. In panel c the red dots indicate BSS when the reference forecast is WRF60 driven by GFS meteorological boundary conditions. (d) BSS of monthly mean AOD from WRF60 (green dots) and WRF12-remap (blue dots) relative to MODIS monthly mean climatology during 2000-2014 (reference forecast). Monthly mean AOD from MODIS are used as the target. BSS for WRF12-remap in September is -6.1.

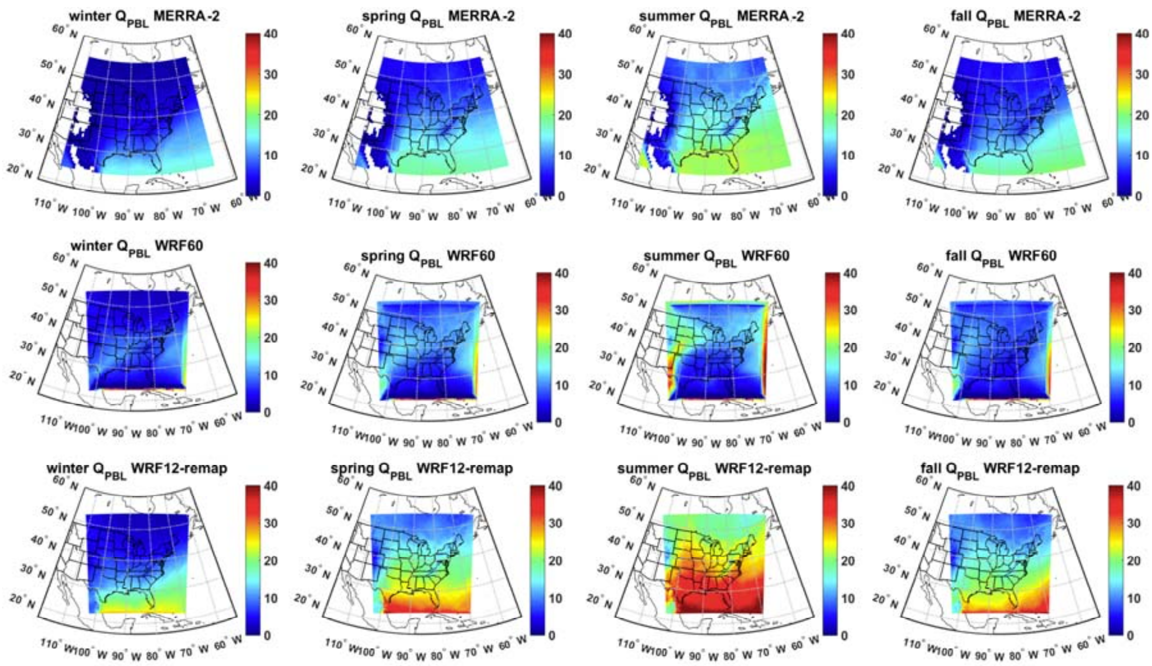

Figure 6. Seasonal mean specific humidity [kg m^{-2}] integrated from the surface to 825 hPa (Q_{PBL}) from MERRA-2 (first row) assuming an average air density in the *PBL* of 1.1 kg m^{-3}, WRF60 (second row), and WRF12-remap (third row). The data are 3-hourly and show only cloud-free hours in all three data sets.

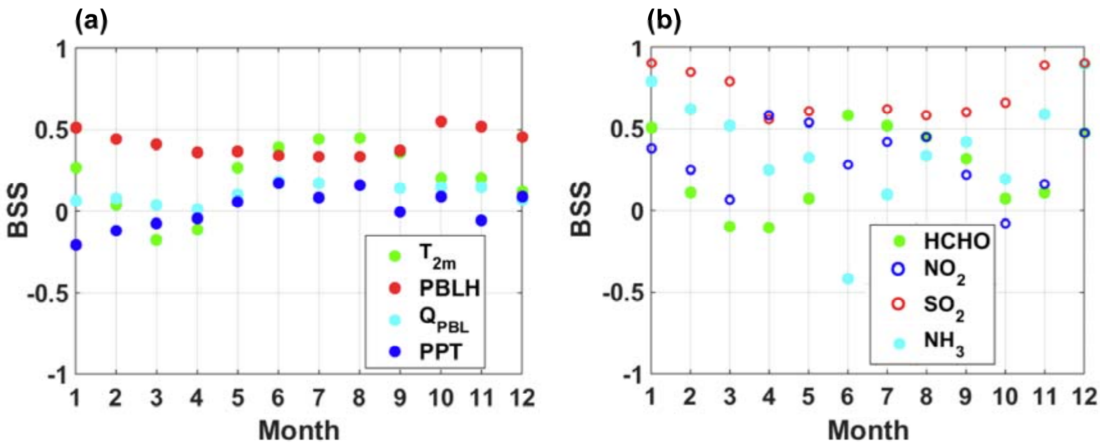

Figure 7. Brier Skill Scores (BSS) for key (a) meteorological and (b) chemical variables. BSS are computed using hourly data of T at 2m (*T_{2m}*) and *PBLH*, 3-hourly estimates of specific humidity in the boundary layer (*Q_{PBL}*), and z-scores of monthly total precipitation (*PPT*), and of monthly mean columnar gas phase concentrations.

Tables

Table 1. Physical and chemical schemes adopted in the WRF-Chem simulations presented herein.

Simulation settings	**Values**
Domain size	300 × 300 (60 × 60) grid points
Horizontal resolution	12 km (60 km)
Vertical resolution	32 levels up to 50 hPa
Timestep for physics	72 s (300 s)
Timestep for chemistry	5 s
Physics option	**Adopted scheme**
Microphysics	WRF Single-Moment 5-class (Hong et al., 2004)
Longwave Radiation	Rapid Radiative Transfer Model (RRTM) (Mlawer et al., 1997)
Shortwave Radiation	Goddard (Fast et al., 2006)
Surface layer	Monin Obhukov similarity (Janjić, 2002;Janjić, 1994)
Land Surface	Noah Land Surface Model (Chen and Dudhia, 2001)
Planetary boundary layer	Mellor-Yamada-Janjich (Janjić, 1994)
Cumulus parameterizations	Grell 3D (Grell and Dévényi, 2002)
Chemistry option	**Adopted scheme**
Photolysis	Fast J (Wild et al., 2000)
Gas-phase chemistry	RADM2 (Stockwell et al., 1990)
Aerosols	MADE/SORGAM (Ackermann et al., 1998;Schell et al., 2001)
Anthropogenic emissions	NEI (2005) (US-EPA, 2009)
Biogenic emissions	Guenther, from USGS land use classification (Guenther et al., 1994;Guenther et al., 1993;Simpson et al., 1995)

Table 2. Spearman correlation coefficients (ρ) between AOD at wavelengths (λ) of 470, 550 and 660 nm from MODIS observations averaged over 12 or 60 km and WRF-Chem simulations conducted at 60 km (WRF60, shown in the table as -60), at 12 km (WRF12, shown in the table as -12), and from WRF-Chem simulations at 12 km but remapped to 60 km (WRF12-remap, shown in the table as -remap). Given WRF12-remap is obtained by averaging WRF12 when at least half of the 5×5 12 km resolution cells contain valid data, ρ from WRF60 and WRF12-remap may be computed on slightly different observations and sample size. The bold text denotes correlation coefficients that are significant at α=0.05 after a Bonferroni correction is applied (i.e. $p \le \frac{0.05}{9 \times 12} = 4.63 \times 10^{-4}$ **is significant). The yellow shading is a visual guide that shows for each month and λ the model output that has highest ρ with MODIS.**

Month→/ Variable↓	Jan	Feb	Mar	Apr	May	Jun	Jul	Aug	Sep	Oct	Nov	Dec
470-12	**0.238**	**0.150**	**0.137**	**0.147**	**0.377**	**0.581**	**0.610**	**0.723**	**0.352**	**0.306**	**0.259**	**0.212**
470-60	0.156	**0.226**	**0.438**	**0.412**	**-0.219**	**-0.146**	**0.379**	**0.601**	0.087	-0.051	**0.500**	-0.059
470-remap	**0.295**	**0.197**	**0.250**	**0.182**	**0.516**	**0.637**	**0.675**	**0.777**	**0.368**	**0.441**	**0.315**	**0.274**
550-12	**0.223**	**0.124**	**0.142**	**0.146**	**0.349**	**0.541**	**0.580**	**0.689**	**0.275**	**0.301**	**0.280**	**0.215**
550-60	**0.179**	**0.244**	**0.429**	**0.332**	**-0.288**	**-0.188**	**0.324**	0.567	0.073	-0.077	**0.491**	0.002
550-remap	**0.297**	0.164	**0.261**	**0.199**	**0.493**	**0.605**	**0.651**	**0.747**	**0.286**	**0.437**	**0.352**	**0.309**
660-12	**0.217**	**0.136**	**0.165**	**0.152**	**0.324**	**0.476**	**0.540**	**0.644**	**0.183**	**0.290**	**0.292**	**0.221**
660-60	**0.191**	**0.230**	**0.437**	**0.402**	**-0.305**	**-0.189**	**0.389**	**0.616**	0.099	**-0.137**	**0.536**	0.049
660-remap	**0.356**	**0.211**	**0.289**	**0.208**	**0.480**	**0.624**	**0.669**	**0.772**	**0.371**	**0.432**	**0.393**	**0.368**

Table 3. Spatial coherence in the identification of extreme AOD values (i.e. areas with AOD>75th percentile over space for each month) between WRF-Chem at different resolutions relative to MODIS. No significant wavelength dependence is found for model skill in identifying extreme AOD so results are only shown for λ = 550 nm. The different model output is denoted by -60 for simulations at 60 km, -12 for simulations at 12 km resolution, and as –remap for simulations at 12 km but with the output remapped to 60 km. The *Accuracy* (Acc) indicates the fraction of grid cells co-identified as extremes and non-extremes between WRF-Chem and MODIS relative to the total number of cells with valid data. The *Hit Rate* (*HR*) is the probability of correct forecast and is the proportion of cells correctly identified as extremes by both WRF-Chem and MODIS. The yellow shading indicates the model resolution with highest skill in each month for AOD at 550 nm.

Month→/ Metric↓	Jan	Feb	Mar	Apr	May	Jun	Jul	Aug	Sep	Oct	Nov	Dec
Acc-12	0.673	0.665	0.659	0.638	0.710	0.800	0.855	0.839	0.666	0.679	0.723	0.661
Acc-60	0.707	0.778	0.735	0.730	0.600	0.587	0.658	0.769	0.661	0.637	0.729	0.681
Acc-remap	0.674	0.680	0.694	0.640	0.766	0.824	0.887	0.837	0.667	0.699	0.767	0.641
HR-12	0.346	0.331	0.319	0.275	0.421	0.599	0.711	0.678	0.333	0.358	0.447	0.323
HR-60	0.417	0.558	0.471	0.460	0.200	0.173	0.315	0.538	0.321	0.274	0.458	0.364
HR-remap	0.350	0.361	0.387	0.281	0.532	0.649	0.775	0.674	0.333	0.399	0.535	0.284

Supplementary Materials for the manuscript:

The impact of resolution on meteorological, chemical and aerosol properties in regional simulations with WRF-Chem

~~Value-added by high-resolution regional simulations of climate-relevant aerosol properties~~

P. Crippa[1], R. C. Sullivan[2], A. Thota[3], S. C. Pryor[2,3]

[1] COMET, School of Civil Engineering and Geosciences, Cassie Building, Newcastle University, Newcastle upon Tyne, NE1 7RU, UK

[2] Department of Earth and Atmospheric Sciences, Bradfield Hall, 306 Tower Road, Cornell University, Ithaca, NY 14853, USA

[3] Pervasive Technology Institute, Indiana University, Bloomington, IN 47405, USA

Table S1. Ratio of spatial variability (i.e. the standard deviation of AOD computed across all grid cells) between AOD at wavelengths (λ) of 470, 550 and 660 nm from MODIS observations mapped at 60 km and WRF-Chem simulations conducted at 60 km resolution (WRF60, shown in the table as -60), at 12 km resolution (WRF12, shown in the table as -12), and from WRF-Chem simulations at 12 km but remapped to 60 km (WRF12-remap, shown in the table as -remap). Given WRF12-remap is obtained by averaging WRF12 when at least half of the 5×5 12 km resolution cells contain valid data, the ratio of standard deviations from WRF60 and WRF12-remap may be computed on slightly different observations and sample size. The yellow shading shows for each month and λ the model with ratio of standard deviations closer to 1.

Month→/ Variable↓	Jan	Feb	Mar	Apr	May	Jun	Jul	Aug	Sep	Oct	Nov	Dec
470-12	0.489	0.581	0.382	0.595	0.806	0.802	1.033	1.20	1.935	1.698	0.766	0.457
470-60	0.615	0.717	0.682	0.648	0.556	0.331	0.353	0.291	0.541	0.605	0.562	0.564
470-remap	0.522	0.630	0.380	0.644	0.993	0.791	1.018	1.194	2.079	2.099	0.853	0.512
550-12	0.406	0.475	0.307	0.480	0.630	0.690	0.996	1.106	1.709	1.401	0.663	0.370
550-60	0.578	0.663	0.629	0.624	0.502	0.302	0.327	0.274	0.480	0.525	0.518	0.505
550-remap	0.431	0.503	0.299	0.524	0.764	0.693	0.990	1.110	1.872	1.758	0.745	0.396
660-12	0.401	0.454	0.283	0.462	0.571	0.671	1.004	1.114	1.684	1.343	0.665	0.351
660-60	0.458	0.531	0.497	0.462	0.378	0.214	0.225	0.184	0.328	0.391	0.402	0.405
660-remap	0.342	0.393	0.235	0.391	0.553	0.474	0.676	0.777	1.369	1.331	0.557	0.307

Table S2. Spatial coherence in the identification of hourly precipitation between WRF-Chem at different resolutions relative to MERRA-2. The Hit Rate (*HR*) indicates the probability of correct forecast and is the proportion of cells correctly identified as with precipitation by both WRF-Chem and MERRA-2. The Mean Fractional Bias (MFB) in space is also reported for each month and computed from the hourly precipitation rates. The yellow shading indicates the model resolution with highest HR and lower absolute MFB in each month for precipitation.

Month→/ Metric↓	Jan	Feb	Mar	Apr	May	Jun	Jul	Aug	Sep	Oct	Nov	Dec
HR-60	0.344	0.298	0.228	0.122	0.083	0.072	0.057	0.059	0.067	0.078	0.154	0.218
HR-remap	0.698	0.715	0.680	0.539	0.402	0.440	0.479	0.438	0.438	0.454	0.581	0.666
MFB-60	-0.340	-0.347	-0.384	-0.442	-0.462	-0.468	-0.475	-0.474	-0.469	-0.459	-0.423	-0.385
MFB-12	-0.095	-0.068	-0.065	-0.168	-0.273	-0.269	-0.260	-0.274	-0.281	-0.261	-0.170	-0.119

Figure S1. Seasonal mean of hourly temperature at 2 meters [K] from MERRA-2 (first row), WRF60 (second row), and WRF12-remap (third row), for simultaneous data from all three datasets.

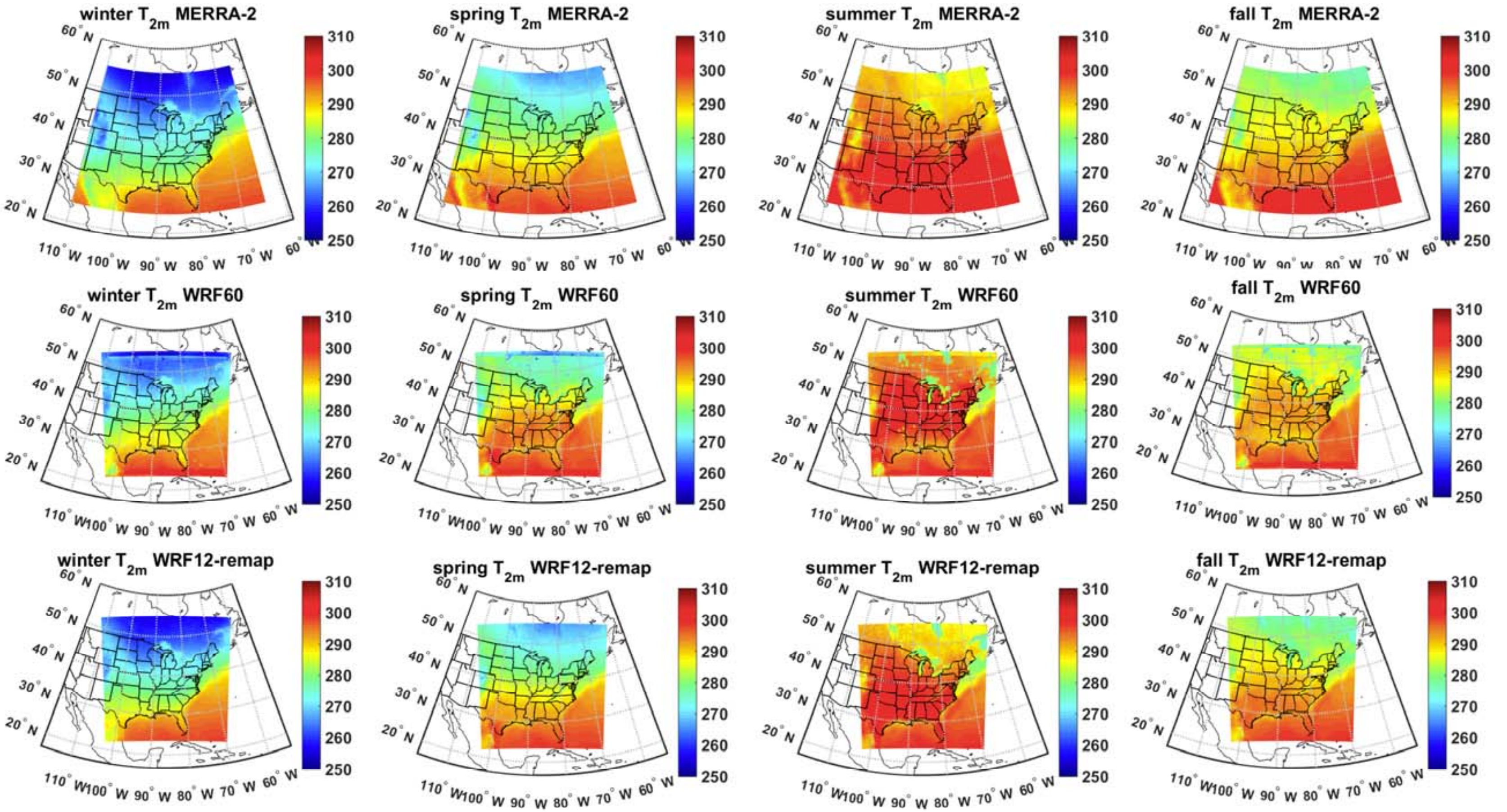

Figure S2. Seasonal average of hourly Planetary Boundary Layer Height, *PBLH* [m] from MERRA-2 (first row), WRF60 (second row), and WRF12-remap (third row), for simultaneous hours of the three datasets.

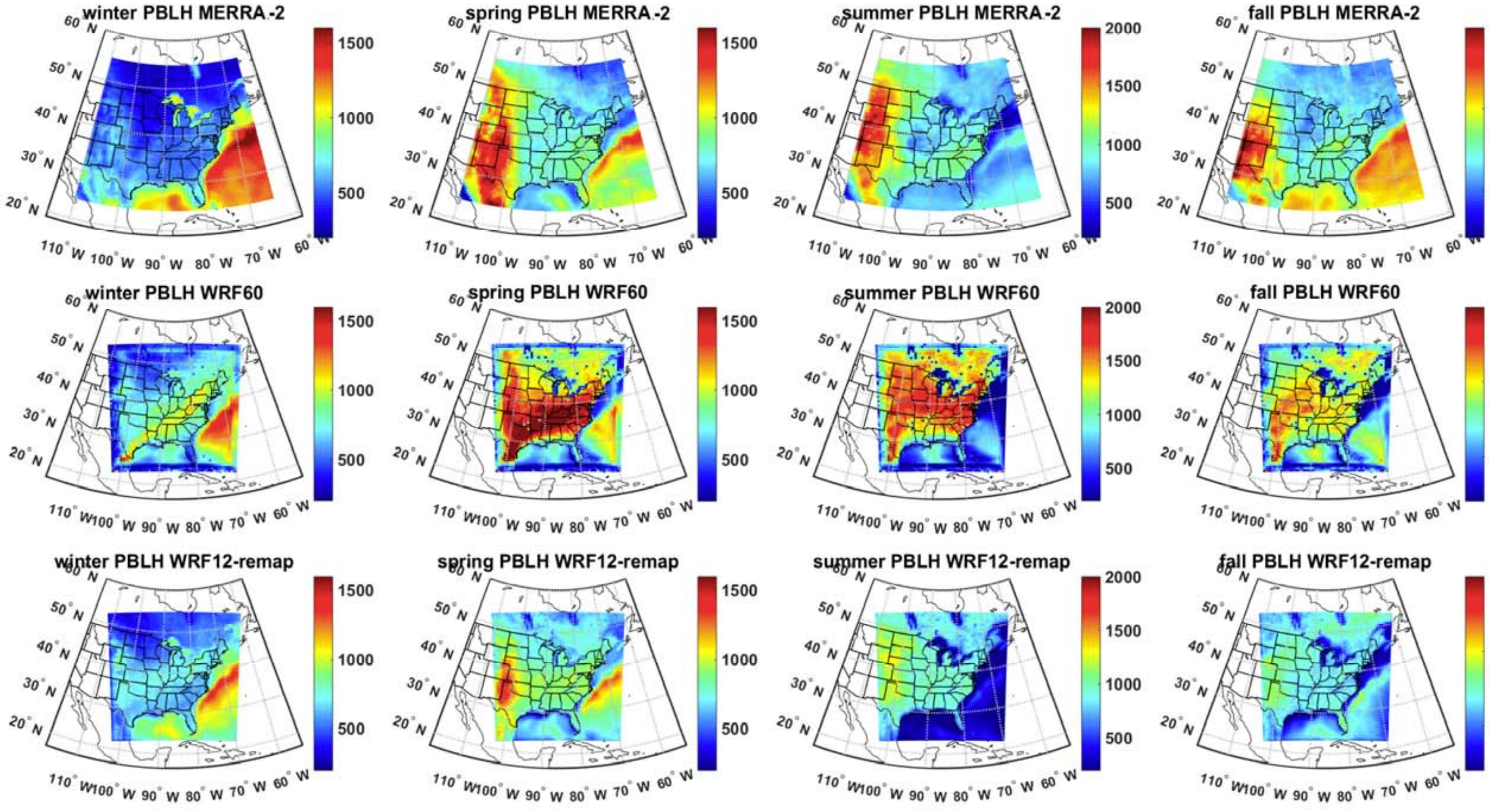

Figure S3. Seasonal total precipitation (mm) from MERRA-2 (first row), WRF60 (second row), and WRF12-remap (third row).

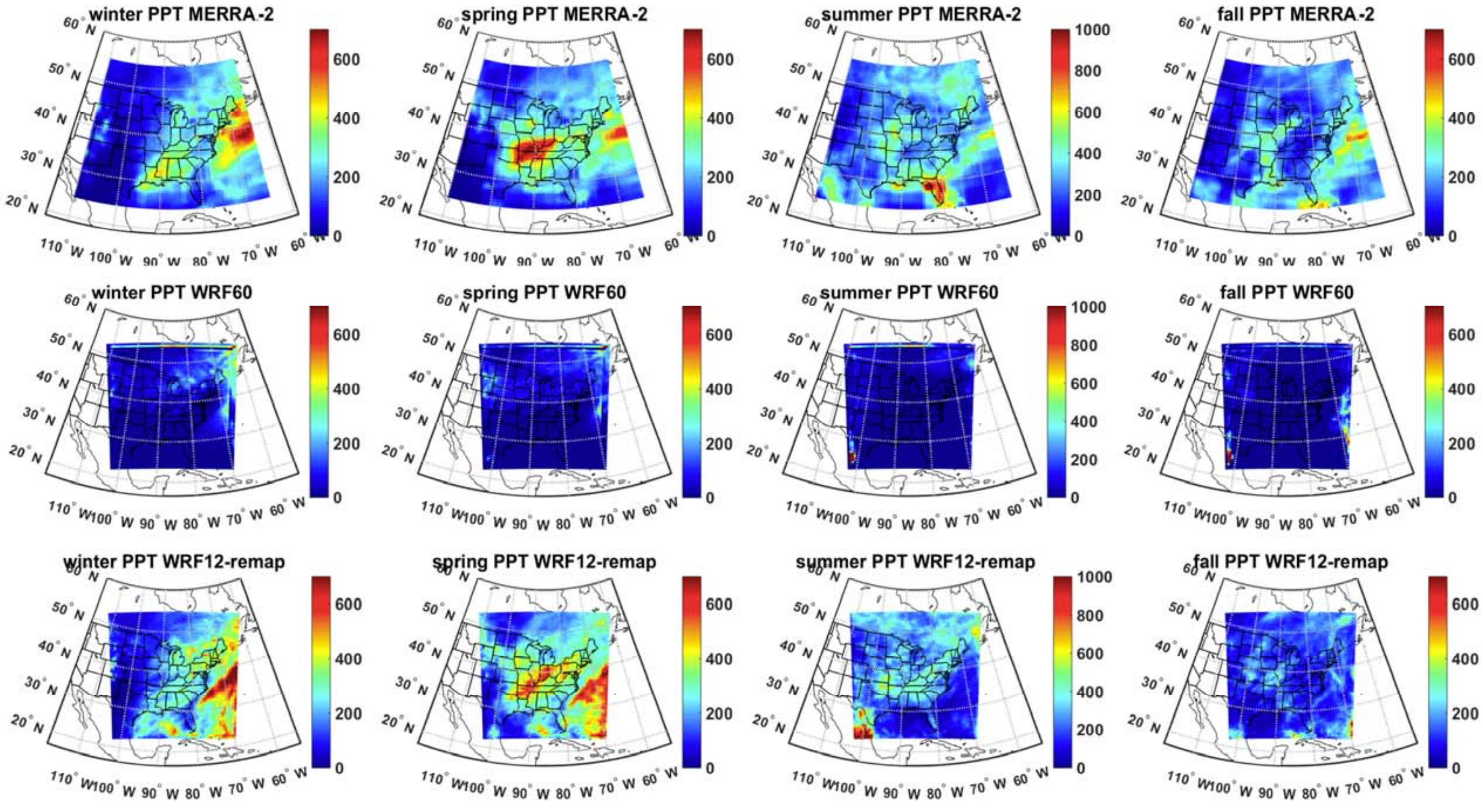

Figure S4. Seasonal total column SO_2 z-scores from OMI (first row), WRF60 (second row), and WRF12-remap (third row). z-scores are computed relative to the spatial seasonal mean of each dataset and indicate the distance from the mean in terms of standard deviation units. A cloud screen of 0.3 is applied to both satellite observations and simulated values. Only grid cells with at least 5 valid observations in a month are used to compute a mean value, otherwise the grid cell is shown as white.

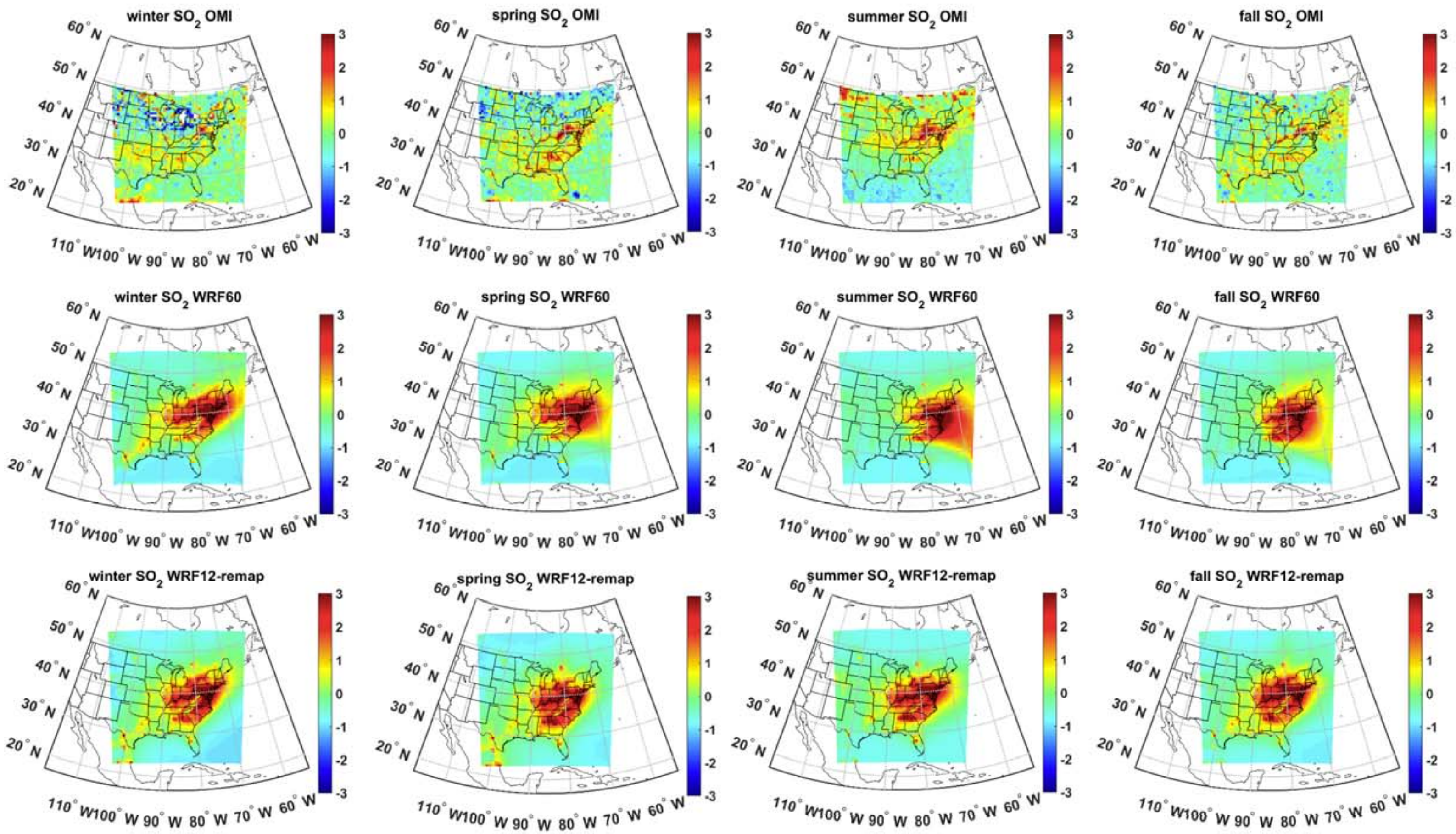

Figure S5. Seasonal total column NO_2 z-scores from OMI (first row), WRF60 (second row), and WRF12-remap (third row). z-scores are computed relative to the spatial seasonal mean of each dataset and indicate the distance from the mean in terms of standard deviation units. A cloud screen of 0.3 is applied to both satellite observations and simulated values. Only grid cells with at least 5 valid observations in a month are used to compute a mean value, otherwise the grid cell is shown as white.

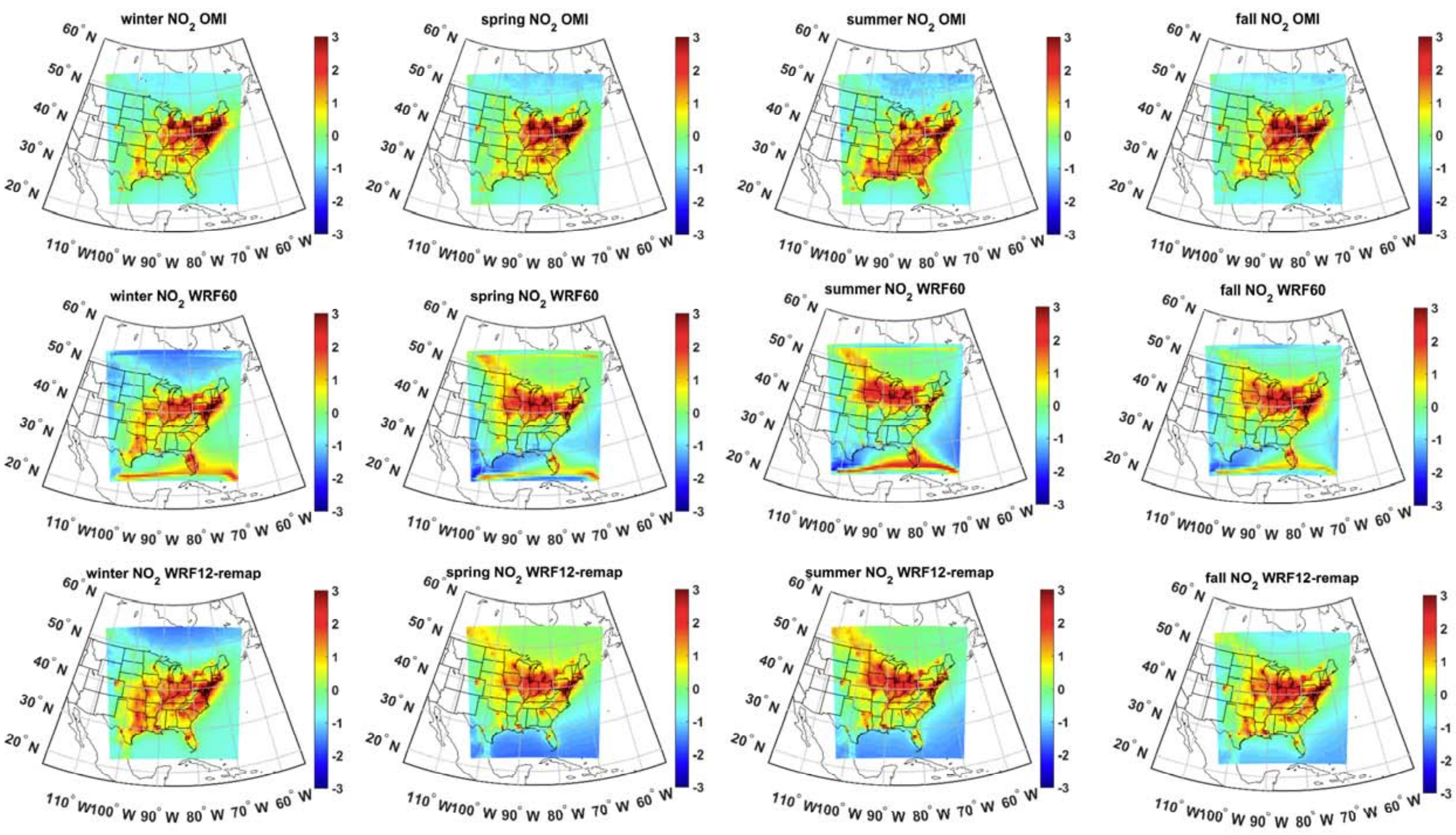

Figure S6. Seasonal total column NH_3 z-scores from OMI (first row), WRF60 (second row), and WRF12-remap (third row). z-scores are computed relative to the spatial seasonal mean of each dataset and indicate the distance from the mean in terms of standard deviation units. A cloud screen of 0.3 is applied to both satellite observations and simulated values. Only grid cells with at least 5 valid observations in a month are used to compute a mean value, otherwise the grid cell is shown as white.

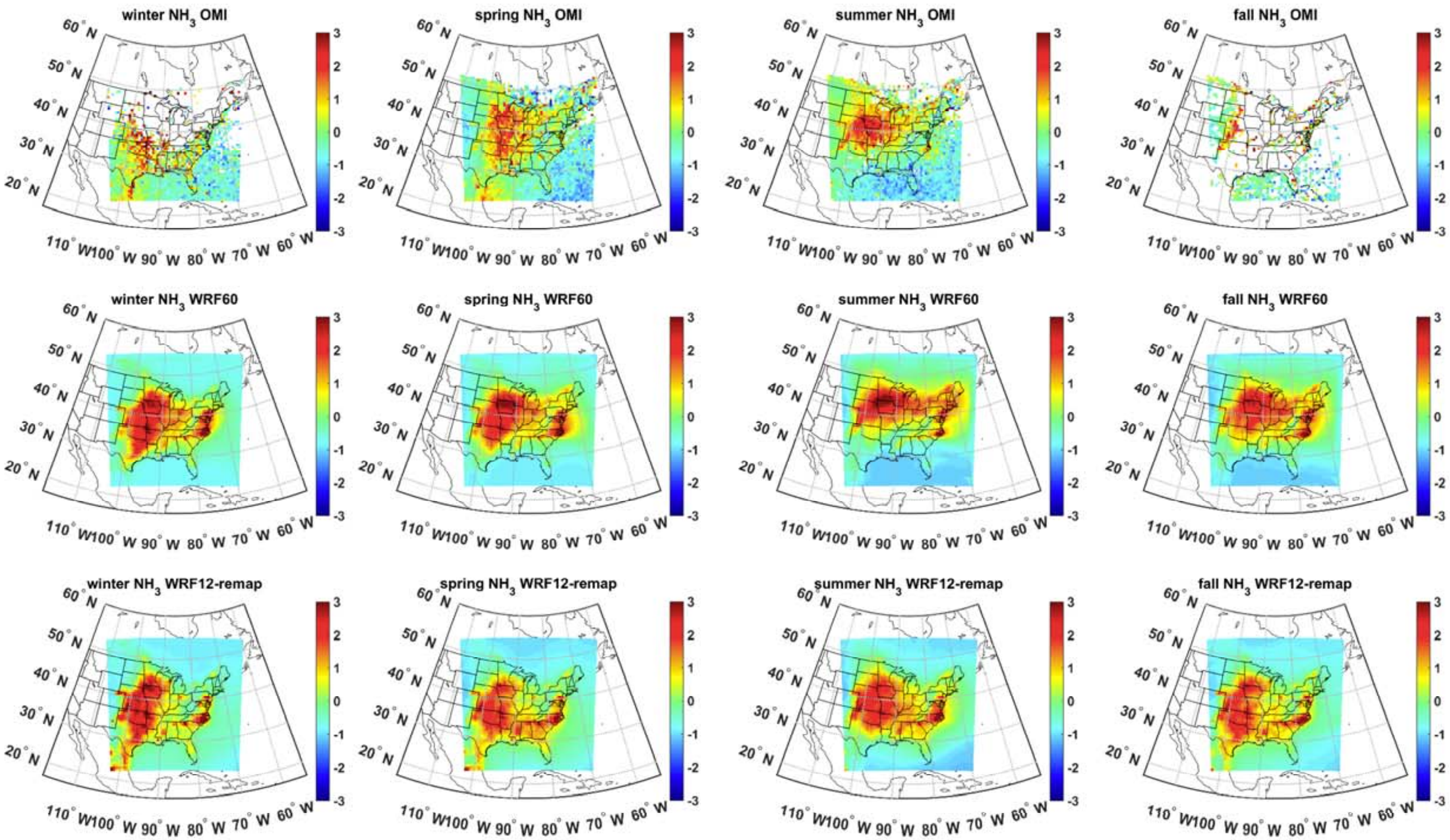

Figure S7. Seasonal total column HCHO z-scores from OMI (first row), WRF60 (second row), and WRF12-remap (third row). z-scores are computed relative to the spatial seasonal mean of each dataset and indicate the distance from the mean in terms of standard deviation units. A cloud screen of 0.3 is applied to both satellite observations and simulated values. Only grid cells with at least 5 valid observations in a month are used to compute a mean value, otherwise the grid cell is shown as white.